Generation of ultrashort laser pulses through filamentation

Master Thesis
by
Anna Engqvist

Lund Reports on Atomic Physics, LRAP-357
Lund, May 2006

Abstract

In this Master Thesis, pulse compression through filamentation has been studied. The method is based on self-focusing of intense laser light in a noble gas like argon. The subsequent plasma formation is used to guide the light over several Rayleigh ranges and hereby to achieve a spectral broadening. In combination with chirped mirrors, the emerging pulses can be compressed to a duration close to the fundamental limit.

The Thesis focuses on the temporal aspects of filamentation. The theoretical part aimed at investigating the different effects involved and the experimental part at implementing and optimising the technique. The best result was a 12.2 fs pulse, for an input of 40 fs.

Acknowledgements

The work of this Master Thesis could not have been performed without the support and inspiration from a number of people, to who I am truly grateful. First of all I would like to thank my supervisor, Professor Anne L'Huillier, for all her help and guidance in writing this Thesis and for the always inspiring discussions. I would also like to thank everybody at the division of Atomic Physics for creating a nice working environment, especially the people in the "Attosecond Physics & High-Order Harmonic Generation" research group, whom I really enjoyed working with. Katalin Varjú, for being my co-supervisor and helping me a lot with the laboratory work. Thierry Ruchon, for working with me on the filament-setup and for his never-ending patience in answering all of my questions. Per Johnsson, for being more or less my reference book when it came to solving (at least to my mind) tricky Matlab-problems. Also with an amazing patience. Johan Mauritsson, who I more or less got to know through his Matlab-code, for helping me with my simulations and also with a lot of the illustrations in this Thesis. Erik Gustafsson, for working with me on the filament-setup and helping me with my Thesis in general. Thomas Remetter, for all the fun discussions and help in general. I am also very grateful to Anders Persson and Emilie Pourtal for helping me with the laser. Besides the people at Lund Institute of Technology, I would like to thank Rodrigo López-Martens and Christoph Hauri at Laboratoire d'Optique Appliquée for learning me a lot about filamentation and for being true sources of inspiration.

Finally, I would really like to thank my friends and family for always supporting me and for having had to put up with my endless monologues about filamentation during the past year. Emelie, without your friendship the time at Lund Institute of Technology would have been so much harder and not half as fun! Rebecca, for supporting me a lot during my Thesis and for all the fun (and not always so very serious) discussions in the lunch room... Last but not least, mum and dad, for always being there and encouraging me in my work.

Contents

Chapter 1

Introduction

The invention of the laser in the 1960s opened up a whole new world of possibilities for scientists all over the world, pushing the limits of monochromaticity, coherence, directionality and brightness. Today, one field of active research is generation of ultrashort pulses, with a wide variety of applications. A recently developed technique is based on self-guidance of laser light in a plasma channel - so called *filamentation* - the subject of this Master Thesis.

1.1 The need for short pulses

Many fundamental processes occur on a pico- or femtosecond time scale (1 ps $= 10^{-12}$ s, 1 fs $= 10^{-15}$ s), so called *ultrafast* processes. Such fast phenomena often concern energy transfer and have mainly been studied in the liquid or solid phase. Examples of ultrafast processes are the photosynthesis together with other chemical reactions that involve dissociation or formation of new molecules. To be able to perform time-resolved measurements of ultrafast processes, pulses less or equal to the duration of the process of study are required. This calls for generation of short or even *ultrashort* ($<$ 1 ps) optical pulses.

An additional driving force is the study of ultra-intense light-matter interactions. Short pulses enable an increase of the peak power of the laser light, without having to increase the pulse energy. There are a number of different techniques to produce short pulses and new ones are constantly developing. In the next section some of the methods most relevant for this Thesis will be presented.

1.2 Generation of high-intensity short laser pulses

The generation of high-intensity short laser pulses uses the technique of *mode-locking*, together with *chirped-pulse amplification (CPA)*. The pulses can also be sent through an external compression stage to become even shorter. There exists a number of different external pulse compression techniques, the most recent being filamentation.

1.2.1 Generation and amplification

In order to generate short pulses directly in the laser oscillator, the active medium must have a broad gain profile to be able to simultaneously support many longitudinal modes and also be resistive to heat. The medium capable of producing the shortest pulses today is a crystal consisting of sapphire doped with three times ionised titanium-atoms, Ti^{3+}:Al_2O_3. Under ordinary circumstances, the phases of the longitudinal modes have random values and a cw oscillation beam will show a random time behaviour [1]. If the phase difference between consecutive longitudinal modes instead is kept constant (locked), the modes oscillate in phase. As a result, short pulses can be obtained according to the *time-bandwidth product*

$$\Delta\omega\Delta t \geq 2\pi c_B \tag{1.1}$$

c_B denotes a constant, whose value depends on the shape of the pulse [2]. With the technique of mode-locking, it is possible to obtain pulses with a duration in the fs-regime and with a peak power in the GW-TW range [3]. Mode-locking can be either active, where an external device produces the desired effect, or passive, which basically uses the inherent properties of some kind of medium. One passive method that has been extensively used is *Kerr-lens mode-locking*, see [4].

To reach even higher power levels, a substantial amplification is needed. If conventional amplifiers are used, the diameter of the beam has to be considerably increased in order not to damage the optical components. As such systems often tend to be both expensive and have low repetition rates, the CPA-technique has emerged. CPA is most easily described in connection with figure 1.1. To reduce the intensity of the laser light without having to expand the beam diameter, the pulse is instead stretched in time by typically a factor of a few thousand. This is accomplished by sending it through a stretcher device, for example consisting of a lens and a grating arrangement, which separates the different frequency components of the pulse. The low-frequency components are then made to travel a shorter distance than the high-frequency components and will thus appear in the leading edge of the pulse, prolonging it in time.

After the pulse has been stretched, it can be amplified. Because of the long pulse duration, the peak power can be kept low and thus a small beam diameter (typically 5 mm) can be maintained. The amplified beam is then expanded to a larger diameter and finally recompressed in time to its original duration. The compressor consists of two gratings and is based on the same principle as the stretcher, in the sense that different frequency components gets to travel different distances. The action of the compressor compensates for the action of the stretcher and thus all the frequency components will exit at the same time, resulting in a recompressed pulse. Since the energy of the pulse has been increased, the peak power is now higher than before the stretching [5].

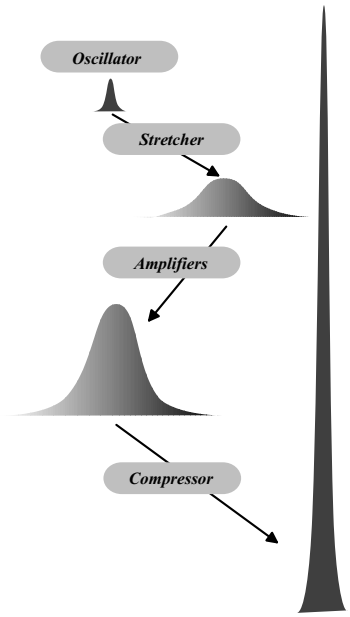

Figure 1.1: Schematic overview of the different steps involved in CPA [6].

1.2.2 External techniques

To further compress the pulses from the laser, external devices must be used, all of which are based on first achieving a spectral broadening of the input pulse and then to compress it temporally, in accordance with the time-bandwidth product. For high enough intensities of the laser light, the refractive index of a medium will start to show a nonlinear intensity dependence, $n = n(I)$. If a Taylor expansion of n versus I is performed, the first term will be proportional to I according to [7]:

$$n = n_0 + n_2 I \tag{1.2}$$

where n_0 denotes the usual linear refractive index and n_2 is the nonlinear coefficient of the medium. This is often denoted *nonlinear refraction*. Since the intensity varies across the pulse, different parts will experience a different refractive index, with a resulting spectral broadening. However, the refractive index is also frequency dependent, $n = n(\omega)$, meaning that different parts of the pulse will propagate with different speeds. This will either prolong or shorten the pulse temporally. To be able to compress the pulse, the nonlinear and dispersive effects of the medium must balance each other and to accomplish this, the cross section of the laser beam must be quite small over a certain distance. Hence some kind of external guiding device is necessary. The first technique was established in 1984, when Tomlinson *et al.* showed that it was possible to compress laser pulses with optical fibres and gratings [8]. This technique could however only compress pulses with an energy of a few nJ, since the material otherwise was destroyed. As one of the primary aspects in producing short laser pulses is to obtain high peak powers, the method had to be improved. In 1996 Nisoli *et al.* presented a method in which a gas-filled hollow waveguide, a capillary, was used instead of an optical fibre [9]. In this way, the energy could be increased and higher peak powers were obtained.

Pulse compression through filamentation has a lot in common with the gas-filled capillary, except that it is based on *self-guidance* of the light in a plasma channel (also known as a filament) and hence requires no constraining device [10]. The technique works both with and without a final recompression stage, due to *self-shaping* of the pulse inside the filament (see section 3.4.1), and pulses as short as 5.1 fs have been produced [11]. The medium used is generally a noble gas like argon [12], but the method also works in air. Compared to the capillary, filamentation circumvents the problems associated with coupling light into the capillary and the compressed pulses have higher energy. Spatially, a filament looks like a glowing, thin thread and is the result of an interplay between two counteracting effects - one focusing and one defocusing. If the two contributions are of equal strength, the radius of the laser beam can be kept more or less constant over a certain distance. The light is thus guided in the same way as a flash of lightning during a thunderstorm. The formation of a filament is usually characterised by three different steps [13]:

1. Focusing of the light in the diffraction plane, caused by *the optical Kerr-effect*. As the intensity of the laser light increases, the refractive index will be intensity dependent according to equation (1.2). Since the spatial intensity profile of laser light in general has its maximum on the optical axis, the refractive index will also exhibit the highest value there. The

medium thus will act as a successively increasing positive lens, so called *self-focusing*.

2. The formation of a plasma due to the increased intensity, creating a filament which is preserved for several Rayleigh ranges. The plasma diffracts the light and hence counteracts the self-focusing.

3. The plasma contribution eventually exceeds the Kerr-effect, causing a final diffraction of the light and the end of the filament.

The exact radius of the filament is not constant throughout the whole propagation, but consists of a number of focusing/defocusing stages due to a very precise interplay between self-focusing and plasma diffraction. Depending on the relative strength of the two physical processes, the radius of the filament will either decrease (dominating Kerr-effect), increase (dominating plasma effect) or be constant (equal strengths of the two contributions).

The physics behind the spatial part of filamentation is rather straightforward. The propagation of the light is governed by the relative strength of two effects, which is controlled by the intensity. But since this quantity not only varies spatially but also temporally, I=I(t), the temporal aspects of filamentation must also be considered. This has been the focus of this Master Thesis.

1.3 Purpose of this Master Thesis

The purpose of this Master Thesis was to study the temporal aspects of filamentation. The theoretical part of the work aimed at investigating the different mechanisms involved and how they affect the temporal and spectral properties of the pulse. For that purpose a one-dimensional propagation code in Matlab was written, that numerically simulates how the temporal and spectral profiles of the pulse are changed as it propagates in the filament. In the experimental part, the theoretical knowledge was used to study the parameter dependence and try to optimise the technique. The aspiration was to obtain as short pulses as possible, with the maximum output energy. The outline of the Thesis is as follows: Chapter 2 is theoretical and covers the different temporal effects involved in filamentation. Chapter 3 describes the numerical method used in the simulations, together with some results and conclusions. Chapter 4 summarises the experimental work, also with results and conclusions. Finally, chapter 5 provides some future aspects and applications of filamentation.

Chapter 2

Temporal aspects of filamentation

To be able to theoretically study how an optical pulse is affected as it propagates in a filament, a propagation equation has to be solved. This is derived from Maxwell's equations, which govern the properties of all electromagnetic fields. To fully understand the meaning of the different mechanisms, a short description of the mathematical properties of a light pulse is first needed.

2.1 Mathematical description of a light pulse

As is well known ever since the *Treatise on Light* by Christian Huygens in 1690 [14], light can be seen as an electromagnetic wave. A total description of a short pulse includes both spatial and temporal characterisation, but since this Thesis is focusing on the temporal properties of pulse propagation, the spatial dependence will be neglected, i.e. $\mathbf{E}(x,y,z,t) = E(t)$. Experimentally, the quantity most easily measured is the intensity of the pulse, related to the electric field according to:

$$I(t) = \frac{\varepsilon_0 c n |E(t)|^2}{2} \tag{2.1}$$

where ε_0 and c are the permitivity and speed of light in vacuum respectively. n is the refractive index of the medium [15]. Mathematically, the electric field is represented by the complex quantity

$$E(t) = |E(t)| e^{i(\varphi(t)+\varphi_0)} \tag{2.2}$$

where $\varphi(t)$ denotes the *temporal phase* of the pulse and φ_0 the *absolute phase*. Expression (2.2) can be further decomposed according to:

$$\begin{aligned} E(t) &= |E(t)| e^{i(\phi(t)-\omega_0 t)} e^{i\varphi_0} = \\ &= |E(t)| e^{i(\phi(t)+\varphi_0)} e^{-i\omega_0 t} = A(t) e^{-i\omega_0 t} \end{aligned} \tag{2.3}$$

In this way, the rapidly varying carrier wave $e^{-i\omega_0 t}$ is separated from the slowly varying complex envelope $A(t)$. ω_0 represents the carrier frequency of the pulse,

usually chosen close to the center of the spectrum [16]. In equation (2.3), the absolute phase relates the position of the carrier wave to the temporal envelope of the pulse and is also known as the *carrier-envelope-offset* (CEO) phase. One of the many advantages of filamentation is a conserved CEO phase [10].

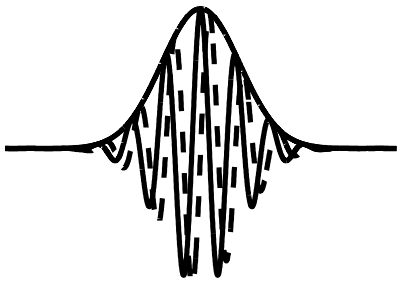

Figure 2.1: The envelope and the electric field of a pulse for two different values of the absolute phase. The solid line represents $\varphi_0 = 0$ and the dashed line $\varphi_0 = \pi/2$ [17].

The instantaneous optical frequency of the electric field varies with the temporal phase according to:

$$\omega(t) = -\frac{d\varphi(t)}{dt} = -\frac{d\phi(t)}{dt} + \omega_0 \tag{2.4}$$

where the minus sign is due to the choice of $e^{-i\omega_0 t}$ in equation (2.3) [18]. If the phase has a nonlinear temporal dependence, the instantaneous optical frequency of the electric field will not be constant but will change with time. The pulse is then said to be frequency modulated or *chirped*. If the frequency of the light increases *linearly* with time, the pulse is referred to as being *positively chirped* or *upchirped* and if the opposite prevails, *negatively chirped* or *downchirped*. Depending on the temporal dependence, the chirp of a pulse can be more or less complicated.

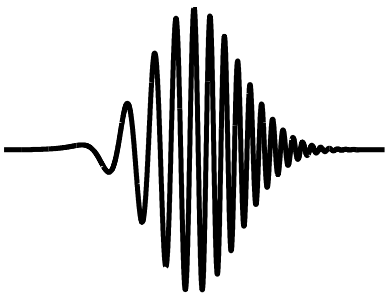

Figure 2.2: The electric field of a pulse with a strong, positive chirp [17].

A complete description of the electric field of a pulse can also be given in the frequency domain, since it is connected to the temporal domain through a Fourier transform. For the same reason as in the temporal domain, a complex

representation of the electric field is often used

$$E(\omega) = |E(\omega)| e^{i\varphi(\omega)} \tag{2.5}$$

with $\varphi(\omega)$ representing the *spectral phase* of the pulse. The spectral phase can be further decomposed by Taylor expansion according to [19]:

$$\begin{aligned} \varphi(\omega) &= \varphi_0 + \sum_{n=1}^{\infty} \frac{1}{n!} a_n (\omega - \omega_0)^n \\ a_n &= \left(\frac{d^n \varphi(\omega)}{d\omega^n} \right)_{\omega=\omega_0} \end{aligned} \tag{2.6}$$

Since the square of the spectral amplitude $|E(\omega)|^2$ represents the spectrum of the pulse, which is very easy to measure experimentally, it is usually more convenient to represent a pulse in the frequency domain. To be able to relate this to the temporal representation, the inverse Fourier transform must be used, since the complex representation of the temporal and spectral electric fields are connected according to:

$$E(t) = \frac{1}{\sqrt{2\pi}} \int_0^{\infty} E(\omega) e^{-i\omega t} d\omega \tag{2.7}$$

By inserting the Taylor expansion of the spectral phase into the expression for the complex electric field, equation (2.5), the resulting exponent looks like:

$$\exp\left\{ i \left[\varphi_0 + \frac{d\varphi}{d\omega}(\omega - \omega_0) + \frac{1}{2}\frac{d^2\varphi}{d\omega^2}(\omega - \omega_0)^2 + \frac{1}{6}\frac{d^3\varphi}{d\omega^3}(\omega - \omega_0)^3 + \ldots \right] \right\} \tag{2.8}$$

If this is inserted into equation (2.7), it can clearly be seen that a linear variation of the spectral phase does not change the temporal profile of the pulse, but instead induces a temporal shift of the entire pulse. A nonlinear phase variation, on the other hand, will cause a frequency chirp in the temporal domain and hence alter the shape of the pulse [19].

Since the temporal and spectral characteristics of an optical pulse are connected, their respective widths will also be linked, in accordance with the time-bandwidth product, see equation (1.1). For a Gaussian pulse, $c_B = 0.441$. Pulses with a duration corresponding to the equality in equation (1.1) are unchirped, i.e. have a constant temporal phase, and hence as short as they can possibly be. Such pulses are therefore referred to as being *transform limited* [2].

As a short ($\sim$ 10 fs), intense laser pulse propagates through a certain medium, it is strongly affected and generally several mechanisms act simultaneously. Basically, these can be divided into *dispersive* and *nonlinear* effects. The temporal and spectral evolution of the pulse inside the filament is governed by a propagation equation, the derivation and explanation of which can be found in appendix A.

2.2 Dispersive effects

2.2.1 Group-velocity dispersion

When a short laser pulse interacts with matter, it will be affected differently depending on the optical frequency of the electric field. Hence different frequency components are influenced by different amounts, a property commonly known as chromatic dispersion, which manifests itself through the frequency dependence of the refractive index, $n(\omega)$. Due to the frequency dependence of the refractive index, the *mode-propagation constant* $\beta = \frac{n(\omega)\omega}{c}$ will also vary with frequency. This will affect the temporal pulse shape. To estimate the effect of dispersion, a Taylor expansion around the center frequency can be performed according to [20]:

$$\begin{aligned} \beta(\omega) &= n(\omega)\frac{\omega}{c} = \beta_0 + \left(\frac{d\beta}{d\omega}\right)_{\omega=\omega_0}(\omega-\omega_0) + \\ &+ \frac{1}{2}\left(\frac{d^2\beta}{d\omega^2}\right)_{\omega=\omega_0}(\omega-\omega_0)^2 + \ldots \end{aligned} \tag{2.9}$$

For short pulses, with broad spectral widths, it is necessary to include higher-order expansions. If the second order expansion $\left(\frac{\partial^2\beta}{\partial\omega^2}\right)_{\omega=\omega_0}$ (also known as β_2) is included, different frequencies will have different *group-velocities*. The group-velocity represents the speed with which the whole pulse travels and should not be confused with the *phase-velocity*; the speed of the separate electromagnetic waves (the different constituents of the pulse). This *group-velocity dispersion* (GVD) alters the temporal characteristics of the pulse. If $\beta_2 > 0$, the phenomenon is referred to as normal (positive) group-velocity dispersion and if $\beta_2 < 0$, anomalous (negative) group-velocity dispersion. For normal dispersion, low-frequency (red-shifted) components of an optical pulse travel faster than high-frequency (blue-shifted) components, while the opposite prevails for anomalous dispersion [21]. Most media exhibit normal dispersion. Because of GVD, the temporal phase varies across the pulse, inducing a chirp. As the frequency changes linearly with time, the chirp is linear. For normal dispersion the chirp is positive, while anomalous dispersion produces a negative chirp. A linear chirp can easily be compensated for by introducing a device with a GVD of opposite sign. In figure 2.3 the effect of GVD is shown.

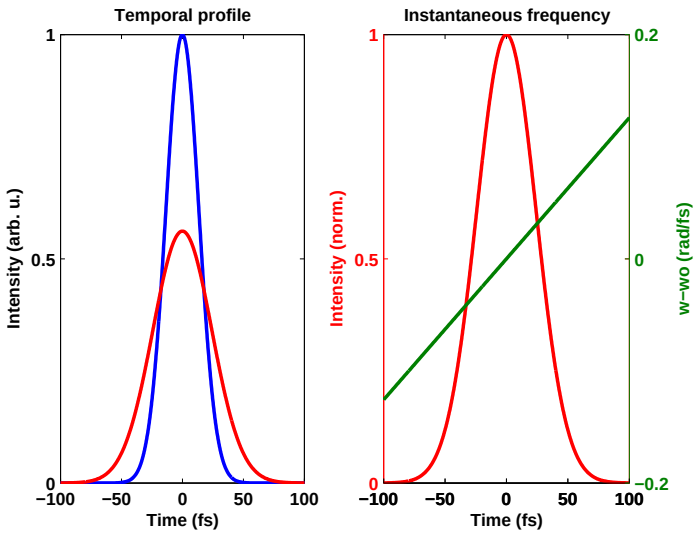

Figure 2.3: Temporal profile of the pulse, together with the frequency variation, before (blue) and after (red) the influence of GVD.

2.2.2 Third-order dispersion

For ultrashort pulses, even the second order of the Taylor expansion is not enough to fully describe the mode-propagation constant, but higher-order terms must also be included. If the next term in the Taylor expansion (2.9) ($\beta_3 = \left(\frac{\partial^3 \beta}{\partial \beta^3}\right)_{\omega=\omega_0}$) is added, the *third-order dispersion* (TOD) is taken into account as well. Unlike GVD, TOD induces an *asymmetric* broadening of the pulse. Depending on the sign of β_3, it makes either the trailing edge ($\beta_3 > 0$) or the leading edge ($\beta_3 < 0$) of the pulse longer and modulated. If the GVD contribution is negligible, the modulation increases. The shape of a pulse that is affected only by TOD, can be seen in figure 2.4 for $\beta_3 > 0$ [22].

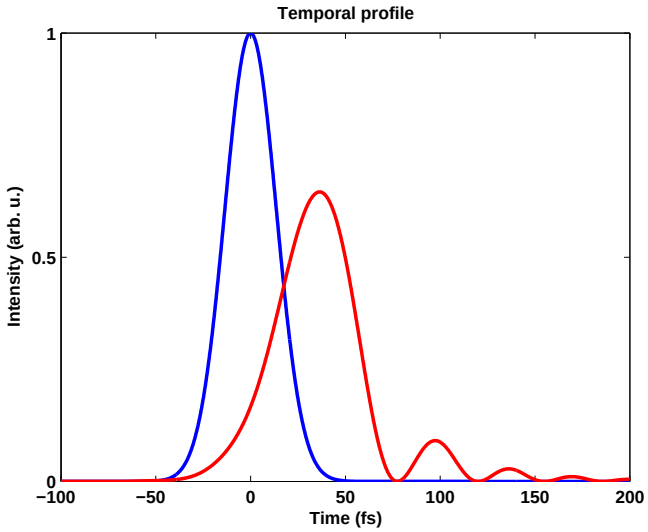

Figure 2.4: Temporal profile of the pulse before (blue) and after (red) the influence of TOD.

2.3 Nonlinear effects

2.3.1 Self-phase modulation

As already mentioned in section 1.2.2, at high intensities the refractive index of a medium starts to show an intensity-dependence, according to:

$$n = n_0 + n_2 I \tag{2.10}$$

Due to the temporal variation of the intensity, the refractive index will also vary in time, which means that different parts of the pulse experience cdifferent responses from the medium [23]. The variation in refractive index causes a self-induced phase shift in the pulse, that increases with propagated distance according to:

$$\begin{aligned} \phi &= \beta z - \omega_0 t = \frac{\omega_0 n(t) z}{c} - \omega_0 t = \\ &= \frac{\omega_0 n_0 z}{c} + \frac{\omega_0 n_2 I(t) z}{c} - \omega_0 t \end{aligned} \tag{2.11}$$

where the intensity-dependent nonlinear phase shift $\phi_{NL} = \frac{\omega_0 n_2 I(t) z}{c}$ is due to nonlinear refraction. Since the instantaneous frequency of the pulse is given by the derivative of the temporal phase, the frequency will also show an intensity- and time-dependence according to:

$$\omega = -\frac{\partial \phi}{\partial t} = \omega_0 - \frac{\omega_0 n_2}{c} \frac{\partial I}{\partial t} z \tag{2.12}$$

It is thus obvious that new frequency components will be generated as the pulse propagates in the medium. Depending on the sign of $\frac{\partial I}{\partial t}$, the spectrum will be either blue- or red-shifted. For the leading edge of the pulse, $\frac{\partial I}{\partial t} > 0$ and the spectrum correspondingly shifts towards the red. For the trailing edge, $\frac{\partial I}{\partial t} < 0$ and the spectrum instead shifts towards the blue. This phenomenon is referred to as *self-phase modulation* (SPM), the temporal counterpart to the optical Kerr-effect.

The spectral broadening due to SPM is associated with an oscillatory structure over the entire frequency range, where the outermost peaks are the strongest. This is easily seen in figure 2.5. Due to the generation of new frequencies as the pulse propagates, SPM induces a chirp in the pulse. Unlike GVD the induced chirp is nonlinear, which makes the pulse impossible to compress [24]. If however SPM and GVD act together on equal footing, a spectral broadening will result at the same time as a linear chirp will be produced. This can be used to compress pulses and is further discussed in section 3.4.1. If normal dispersion prevails, the pulse stretches more rapidly compared to the situation when only GVD is present. This can be explained by the fact that SPM generates red-shifted frequency components at the leading edge of the pulse and blue-shifted at the trailing edge. Since low frequencies travel faster than high for normal dispersion, the pulse shows an enhanced temporal stretching. Due to the decrease in intensity, the SPM-induced phase shift decreases, see equation (2.11). If the dispersion instead is anomalous, the pulse instead initially stretches at a much lower rate than if only GVD was present and eventually reaches a steady state. Since the SPM-induced chirp is positive for the central part of the pulse, while

the dispersion-induced chirp is negative, the two contributions will counteract, thus limiting the temporal stretching of the pulse. Also the broadening of the spectrum is reduced.

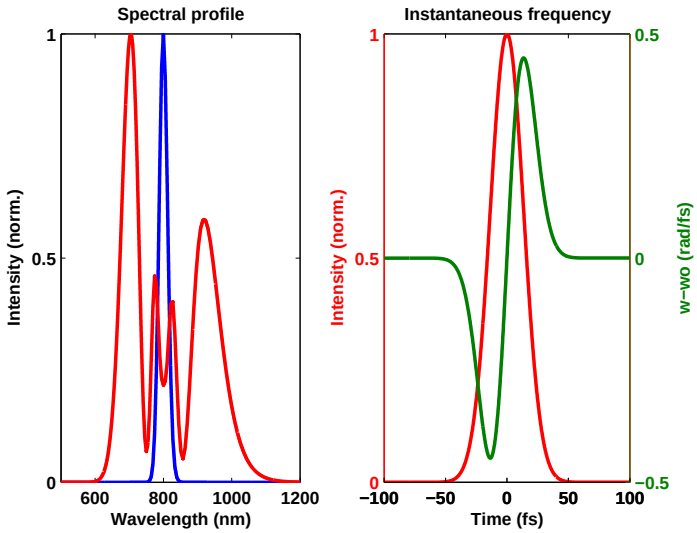

Figure 2.5: Spectral profile of the pulse, together with the frequency variation, before (blue) and after (red) the influence of SPM.

2.3.2 Self-steepening

For ultrashort pulses, it is also necessary to include higher-order nonlinear effects. There are two nonlinear contributions of interest in this context; intrapulse Raman scattering and self-steepening. The first effect has to do with the fact that nonlinear refraction is not instantaneous, but occurs after a certain delay, the so called *response time* of the medium. The change in refractive index of the medium is caused by either electronic polarisation or molecular orientation and depending on which, the response time will be different. The medium used in this Thesis is the noble gas argon, in which molecular orientation is not present. Hence only the electronic polarisation has to be taken into consideration and since its response time is very fast in comparison with the pulse duration in this Thesis, the effect of intrapulse Raman scattering can be neglected.

Self-steepening occurs since the group-velocity of a pulse is intensity-dependent [25]-[28]. The higher the intensity, the lower the group-velocity, which for ultrashort pulses mean that the peak will move slower than the wings. This leads to an asymmetry in the temporal profile, where the trailing edge becomes steeper and steeper. As a result, the SPM-modulated spectrum has a larger broadening on the blue side [29]-[33]. In addition, due to the fact that both SPM and self-steepening act instantaneously, the laser energy is accumulated in the ascending part of the pulse, causing more intense red-shifted peaks [10]. The combined effects of SPM and self-steepening can be seen in figure 2.6.

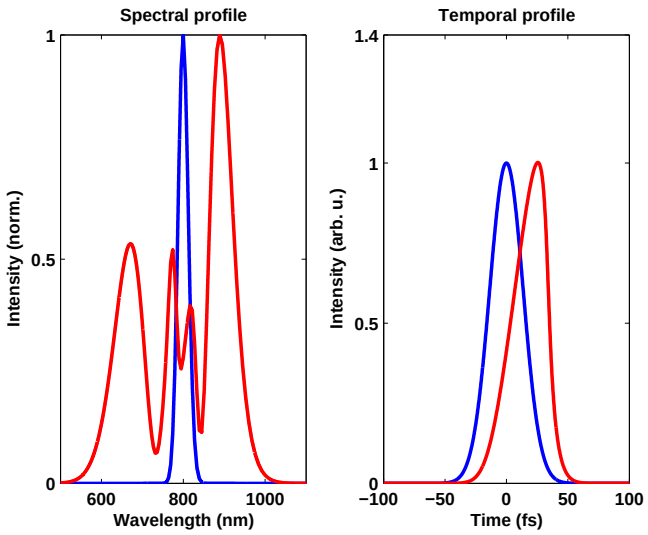

Figure 2.6: Spectral and temporal profiles of the pulse before (blue) and after (red) the influence of SPM and self-steepening.

2.3.3 Plasma generation

As the intensity of the laser light increases due to self-focusing, the atoms of the medium will be ionised (partially or completely) and a plasma is created. If the energy of the individual photons is not sufficient to directly ionise the atoms, i.e. $\hbar\omega < I_p$ where I_p is the ionisation potential of a single atom, the process is called *optical field ionisation* (OFI). Optical field ionisation can be further divided into three different regimes depending on the intensity and frequency of the laser field: *multiphoton ionisation*, *tunneling ionisation* and *over-the-barrier ionisation*. The first two regimes are separated by the *Keldysh parameter* (γ):

$$\gamma = \frac{\omega}{E_{laser}}\sqrt{2I_p} \tag{2.13}$$

where E_{laser} denotes the electric field strength of the laser light [34]. If $\gamma \gg 1$, i.e. for laser fields with high frequencies and/or low intensities, an electron successively will absorb a number of photons, rise to higher energy states and eventually leave the atom. This type of ionisation is therefore called multiphoton ionisation. If, on the other hand, the intensity of the laser field is high enough (so that $\gamma \ll 1$), the potential well in the atom will be deformed. This creates a barrier, through which there is a possibility that the electron can tunnel, thereby leaving the atom. The tunneling process is a pure quantum mechanical concept and has no classical counterpart. Tunneling is the dominating ionisation process for neutral atoms interacting with laser light of 800 nm and an intensity exceeding 10^{14} W/cm^2. For even higher intensities, the atomic potential well is further deformed and the barrier will be suppressed below the ground state. This means that the electron is now in an unbound state, from where it can easily leave the atom [35].

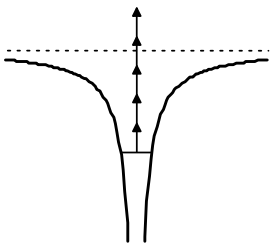

Figure 2.7: Schematic description of multiphoton ionisation [35].

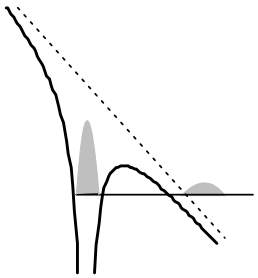

Figure 2.8: Schematic description of tunneling ionisation [35].

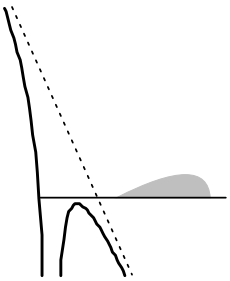

Figure 2.9: Schematic description of over-the-barrier ionisation [35].

As the laser pulse passes and a plasma is created, the properties of the medium change. During the time of the interaction, the matter consists of a varying number of ions, free electrons and neutral atoms, depending on I(t). When the interacting pulse is of femtosecond duration, the heavy ions can be considered immobile while the lighter electrons are easily disturbed by the external field and start to oscillate at the resonance plasma frequency:

$$\omega_p^2(t) = \frac{e^2 n_e(t)}{m_e \varepsilon_0} \tag{2.14}$$

where $n_e(t)$ is the density of free electrons due to ionisation [36]. This in turn affects the refractive index of the medium, that changes according to:

$$\Delta n(t) = -\frac{\omega_p^2(t)}{2\omega_0^2} = -\frac{e^2 n_e(t)}{2 m_e \varepsilon_0 \omega_0^2} \tag{2.15}$$

The time-dependent variation of the refractive index leads to a change in phase, just like SPM:

$$\phi_{Pl} = \Delta k z = k_0 \Delta n z = -k_0 \frac{e^2 n_e(t)}{2 m_e \varepsilon_0 \omega_0^2} z = -\frac{e^2 n_e(t)}{2 m_e \varepsilon_0 \omega_0 c} z \tag{2.16}$$

Here $k_0 = \frac{2\pi}{\lambda}$ represents the propagation constant in vacuum [37]. Since the degree of ionisation increases as the laser pulse passes, the refractive index decreases with time, resulting in a blue-shift of the fundamental spectrum. In addition, in contrast to most materials, the plasma introduces an anomalous dispersion in the laser pulse.

The density of free electrons can be further expressed as:

$$n_e(t) = \sum_k k N_k \tag{2.17}$$

where N_k denotes the density of atoms with charge $-ke$ [37]. If only the outermost electron is ionised, then equation (2.17) reduces to:

$$n_e(t) = N_1 \tag{2.18}$$

During the time of the interaction, the density of atoms changes according to:

$$\begin{aligned} \frac{dN_k}{dt} &= W_{k-1} N_{k-1} - W_k N_k \Longrightarrow \frac{dN_1}{dt} = W_0 N_0 \\ \frac{dN_0}{dt} &= -W_0 N_0 \Longrightarrow N_0 = N_{00} \exp\left[-\int_{-\infty}^{t} W_0\left(t'\right) dt'\right] \Longrightarrow \\ \Longrightarrow \frac{dN_1}{dt} &= W_0(t) N_0(t) = W_0(t) \cdot N_{00} \exp\left[-\int_{-\infty}^{t} W_0\left(t'\right) dt'\right] \end{aligned} \tag{2.19}$$

where W_k represents the ionisation rate of an atom with charge $-ke$ and N_{00} denotes the density of neutral atoms before interaction with the laser light. If this differential equation is solved, the free electron density as a function of time can be written as:

$$n_e(t) = N_{00} \int_{-\infty}^{t} W_0\left(t'\right) \exp\left[-\int_{-\infty}^{t'} W_0\left(t''\right) dt''\right] dt' \tag{2.20}$$

To further calculate this expression, the ionisation rate has to be determined. Since in this Thesis, the atoms are ionised through tunneling, a quantum mechanical treatment is required. The result is merely stated here, for a complete derivation, see appendix A.2. For a linearly polarised, alternating electromagnetic field, the ionisation rate can be written in the following form (in atomic units):

$$W_{ion,linear}\left(\mathscr{E},\omega\right) = \left(\frac{3\mathscr{E}}{\pi\mathscr{E}_0}\right)^{1/2} \times \left|C_{n^*l^*}\right|^2 E \frac{\left(2l+1\right)\left(l+|m|\right)!}{2^{|m|}\left(|m|\right)!\left(l-|m|\right)!}\left(\frac{2\mathscr{E}_0}{\mathscr{E}}\right)^{2n^*-|m|-1} \times \times \exp\left(\frac{-2\mathscr{E}_0}{3\mathscr{E}}\right) \tag{2.21}$$

[38]. Here $\mathscr{E}_0 = (2E)^{3/2}$, $n^* = Z\left(2E\right)^{-1/2}$, E is the electron energy, Z is the charge of the resulting ion and $\mathscr{E}$ is the amplitude of the external field. l and m are the orbital and magnetic quantum number respectively. The factor $\left(\frac{3\mathscr{E}}{\pi\mathscr{E}_0}\right)^{1/2}$ appears from averaging over a period of the external field and $\left(2\mathscr{E}_0/\mathscr{E}\right)^{2n^*-|m|-1}$ is a factor which takes the Coulomb interaction into account. The expression for the dimensionless constant $\left|C_{nl}\right|^2$ is known only for the hydrogen atom, but by applying the asymptotic Stirling formula, it can for an arbitrary atom be written as:

$$\left|C_{n^*l^*}\right|^2 = \frac{1}{2\pi n^*}\left(\frac{4e^2}{n^{*2}-l^{*2}}\right)^{n^*}\left(\frac{n^*-l^*}{n^*+l^*}\right)^{l^*+1/2} \tag{2.22}$$

$n^* = n-\delta_l$ and $l^* = l-\delta_l$ represent the effective quantum numbers, which take the quantum defect $\delta_l = n-\left(2E\right)^{-1/2}$ into consideration [34]. If the expression for $\left|C_{n^*l^*}\right|^2$ is inserted into the expression for the ionisation rate, equation (2.21), it can be seen that the maximum rate is obtained for $|m| = 0$.

Chapter 3

Numerical simulation

3.1 Problem to solve

To theoretically study light propagation in a filament, the following propagation equation has to be solved, including both dispersive and nonlinear effects:

$$\begin{aligned}\frac{\partial U}{\partial z} &= -i\frac{sgn\left(\beta_2\right)}{2L_D}\frac{\partial^2 U}{\partial \tau^2} + \frac{sgn\left(\beta_3\right)}{6L_D^{'}}\frac{\partial^3 U}{\partial \tau^3} + \\ &+ i\frac{1}{L_{NL}}\left[\left|U\right|^2 U + is\frac{\partial}{\partial \tau}\left(\left|U\right|^2 U\right)\right] - i\frac{n_0 n_e\left(t\right)e^2}{2k_0 c^2 m_e \varepsilon_0} \end{aligned} \tag{3.1}$$

The equation is valid for the slowly varying amplitude U of the pulse. The first two terms are due to dispersion (GVD and TOD respectively), the third term is nonlinear (SPM and self-steepening), while the fourth term introduces the effect of the plasma [37]. As stated earlier, $k_0 = \frac{2\pi}{\lambda}$ represents the propagation constant in vacuum and n_0 represents the linear refractive index of the medium. The definition of β_2 and β_3 is found in section 2.2. L_D, $L_D^{'}$ and L_{NL} are length scales, governing the relative importance of the dispersive and nonlinear effects, defined according to:

$$L_D = \frac{T_0^2}{|\beta_2|} \tag{3.2}$$

$$L_D^{'} = \frac{T_0^3}{|\beta_3|} \tag{3.3}$$

$$L_{NL} = \frac{1}{\gamma P_0} \tag{3.4}$$

T_0 denotes the pulse duration ($1/e^2$) and $\gamma = \frac{n_2\omega_0}{cA_{eff}}$ is a nonlinear parameter, where n_2 and A_{eff} represent the nonlinear refractive index of the medium and the effective area of the beam respectively. Finally, P_0 denotes the peak power of the pulse. The parameter s governs the effect of self-steepening [39][40]

$$s = \frac{1}{\omega_0 T_0} \tag{3.5}$$

For a derivation of the part of the equation valid for a neutral medium, see appendix A.

Since equation (3.1) is rather complicated to solve, a numerical approach in most cases is of necessity. There are a number of different methods to numerically simulate how the pulse is affected as it propagates through different media and can be divided into two broad categories known as:

1. Finite-difference methods
2. Pseudospectral methods

In general, pseudospectral methods are faster by up to an order of magnitude, still achieving the same accuracy [41]. The pseudospectral method most commonly used for solving propagation problems in nonlinear dispersive media is the split-step Fourier method [42][43], which has been used in this Thesis. In the following section, the basic aspects of the method will be covered.

3.2 Split-step Fourier method

The split-step Fourier method used in this Thesis, can be rewritten in the rather simple form

$$\frac{\partial U}{\partial z} = \left(\hat{D} + \hat{N}\right) U \tag{3.6}$$

$\hat{D}$ is a differential operator, taking dispersive effects in a linear medium into account, while $\hat{N}$ includes the nonlinear contributions:

$$\hat{D} = -i\frac{sgn\left(\beta_2\right)}{2L_D}\frac{\partial^2}{\partial\tau^2} + \frac{sgn\left(\beta_3\right)}{6L_D^{'}}\frac{\partial^3}{\partial\tau^3} \tag{3.7}$$

$$\hat{N} = i\frac{1}{L_{NL}}\left[|U|^2 + is\frac{1}{U}\frac{\partial}{\partial\tau}\left(|U|^2 U\right)\right] - i\frac{n_0 n_e\left(t\right)e^2}{2k_0 c^2 m_e \varepsilon_0} \tag{3.8}$$

In reality, dispersive and nonlinear effects act simultaneously as the pulse propagates. However, if the propagated distance can be divided into a number of sufficiently small steps h, then the effects can be considered to act independently. This is the basic principle of the split-step Fourier method. The propagation from z to $z+h$ is consequently carried out in two steps. First the nonlinear effects act alone and $\hat{D}=0$ in equation (3.6), then dispersion is considered and $\hat{N}=0$. Mathematically, this is described by:

$$U\left(z+h,t\right) \approx \exp\left(h\hat{D}\right)\exp\left(h\hat{N}\right)U\left(z,t\right) \tag{3.9}$$

To obtain an expression for $\exp\left(h\hat{D}\right)$, the Fourier domain is used

$$\exp\left(h\hat{D}\right)U\left(z,t\right) = F_T^{-1}\left\{\exp\left[h\hat{D}\left(i\omega\right)\right]F_T U\left(z,t\right)\right\} \tag{3.10}$$

where F_T and F_T^{-1} denote the Fourier transform and the inverse Fourier transform respectively. The expression for $\hat{D}\left(i\omega\right)$ is obtained by replacing the operator $\frac{\partial}{\partial\tau}$ in equation (3.7) by $i\omega$, i.e.

$$\hat{D}\left(i\omega\right) = i\frac{sgn\left(\beta_2\right)\omega^2}{2L_D} - i\frac{sgn\left(\beta_3\right)\omega^3}{6L_D^{'}} \tag{3.11}$$

The split-step Fourier method is accurate to the second order in the step size h, i.e. the smaller the steps, the higher the accuracy [44]. The propagation code written in this Thesis is a continuation of a simulation software written by Dr. Johan Mauritsson, see further [45].

3.2.1 Limitations

No numerical simulation exactly reflects a real physical situation, but uses some approximations. In this Thesis, the following approximations have been used:

- The slowly varying field approximation is used, restricting the simulations to pulses longer than ~ 10 fs for the visible and near infrared region [46].
- The simulations only consider one dimension and do not include any spatial effects, like self-focusing and diffraction. In addition, only the *average* pulse intensity is used, ignoring any spatial variations.
- The ionisation rate is considered to be constant in the filament and determined by the input intensity.
- Losses due to absorption have been neglected.

3.3 Simulation overview

The simulation program is written for pulses from the kHz laser system at the Lund High-Power Laser Facility. The specifications, together with a thorough description of the system, are found in section 4.2. To give an overview of how the program runs and to facilitate the interpretation of the results, the simulations can be divided into the following steps, all depicted in figure 3.1:

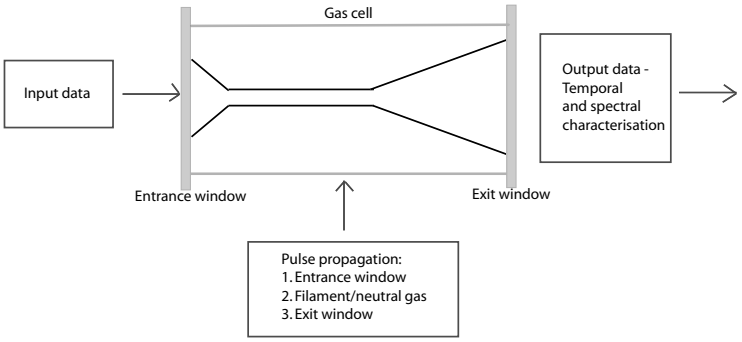

Figure 3.1: Simulation overview.

At first, the main program is provided with all the necessary input data to run a simulation, e.g. the input energy and pulse duration, the data for the different optical components and the pressure in the gas cell. The position and size of the geometrical focus in the gas cell are then calculated. The same setup as in the experimental part has been used, see further section 4.1. After that, the pulse starts to propagate; through the entrance window, self-focuses in the gas and then passes through a filament of variable length. Finally, the

pulse is propagated through the exit window and the effects from the different contributions are plotted.

3.4 Results and discussion

The main purpose of the simulations was to try to understand the physics involved in filamentation (i.e. which effect does what to the pulse) and also investigate how well the process can be described by only considering one dimension. To try to mimic a real filament, the spot size has been varied along the propagation. In each simulation, the following is plotted:

1. The temporal and spectral profiles of the pulse, before and after propagation through a certain part of the setup.
2. The frequency variation across the output pulse.
3. The spectral phase of the output pulse.

The input pulse duration, pulse energy and Ar-pressure are 32 fs, 0.8 mJ and 870 mbar respectively. The light is linearly polarised. This corresponds to typical experimental input parameters.

3.4.1 Self-shaping

Pulse propagation and evolution in a filamentation-setup is governed by a balance between positive and negative dispersion, together with the simultaneous action of nonlinear effects. If the different contributions are exactly balanced, the pulse will be compressed in time and there is no need for chirped mirrors. This has recently been experimentally accomplished by Hauri *et al.* [47]. The pulse first passes through the entrance window of the gas cell, which is made of sapphire and 0.3 mm thick and then self-focuses in the gas. The result is seen in figure 3.2. The combined action of SPM (from the window and the neutral atoms in the gas) and GVD (mainly from the window) produce a temporally and spectrally broadened pulse with a linear, positive chirp over the central parts. The pulse is also affected by self-steepening, tilting the pulse towards the trailing edge. Eventually the intensity gets high enough to ionise the gas and a plasma is created. Inside the filament, the evolution of the pulse is governed by a dynamical interplay between SPM and plasma effects, together with self-steepening. In the early parts of the filament SPM dominates, due to a high number of neutral atoms. Later on, more atoms are ionised, the free electron density increases and the plasma effects become more prominent. Since the two contributions counteract, reducing and flattening the spectral phase, the rough shape of the spectrum is determined by the entrance window and the self-focusing stage. The plasma channel only provides a minor blue-shift to the prior spectrum.

In addition to the above mentioned *nonlinear effects*, the plasma also adds anomalous dispersion to the pulse. This is due to the fact that an increasing density of free electrons decreases the refractive index of the medium. Hence a negative chirp is produced, counteracting the chirp caused by the entrance window and the self-focusing stage, compressing the pulse temporally. Since the amount of dispersion induced is rather high, the temporal profile of the

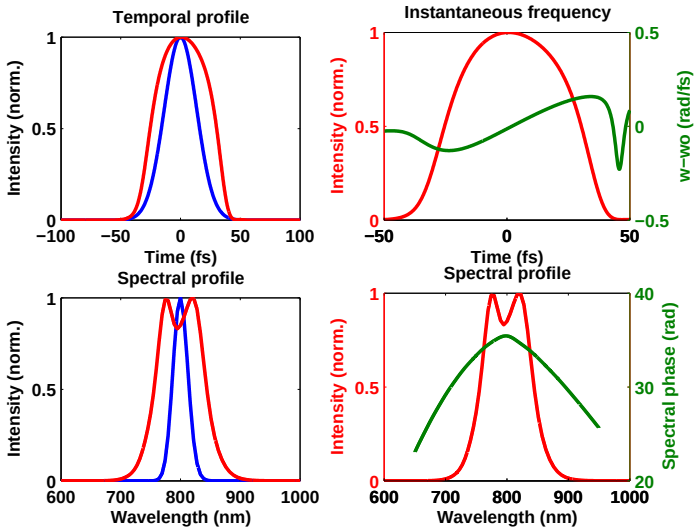

Figure 3.2: Temporal and spectral profiles of the pulse before (blue) and after (red) the entrance window and the self-focusing stage.

pulse will be affected by a comparable amount of GVD and TOD over a longer distance. The result is an oscillating structure near the trailing edge, where the minima do not reach zero. The impact of the filament can be seen in figure 3.3. Here the propagated distance is about 12 cm. To get an optimal effect out of the filament, the contributions from SPM and the plasma must be comparable. SPM alone lacks the necessary negative dispersion, while the plasma itself can not acquire enough spectral broadening (only to the blue, while SPM generates both a red- and a blue-shift). The balance between SPM and plasma contribution is governed by a number of different parameters. The most important being the properties of the cell windows, the input intensity and of course also the pressure of the gas, determining the atomic density.

The pulse finally passes through the exit window of the gas cell. Since the spot size is rather large at this point, due to diffraction caused by the plasma at the end of the filament, the nonlinear effects can be neglected. However, the pulse will be affected by normal dispersion. Since the amount of GVD decreases (opposite sign to the GVD introduced in the filament), the oscillations at the trailing edge reduce. The pulse is also stretched a bit. The final output pulse is seen in figure 3.4. Since the chirp induced by the exit window is positive, it is important to generate a slightly negative chirp in the filament, in order to achieve a chirp-free output pulse. As comparison is also inserted the transform limited output pulse, see figure 3.5. It is clear that the self-shaped pulse is very close to the fundamental limit.

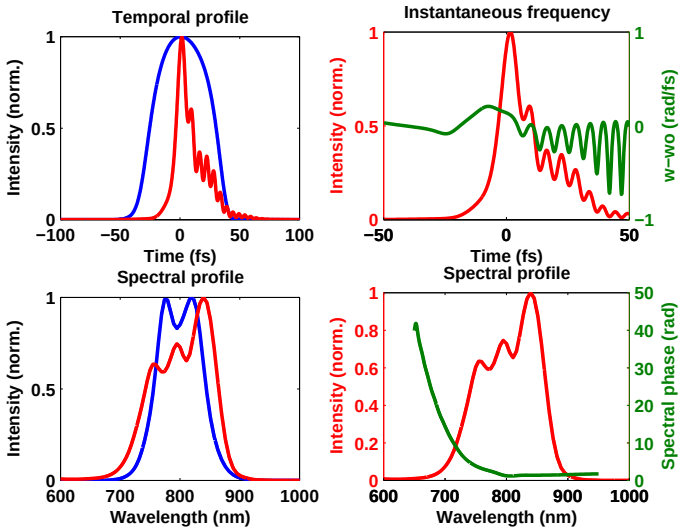

Figure 3.3: Temporal and spectral profiles of the pulse before (blue) and after (red) propagation in a 12 cm long filament.

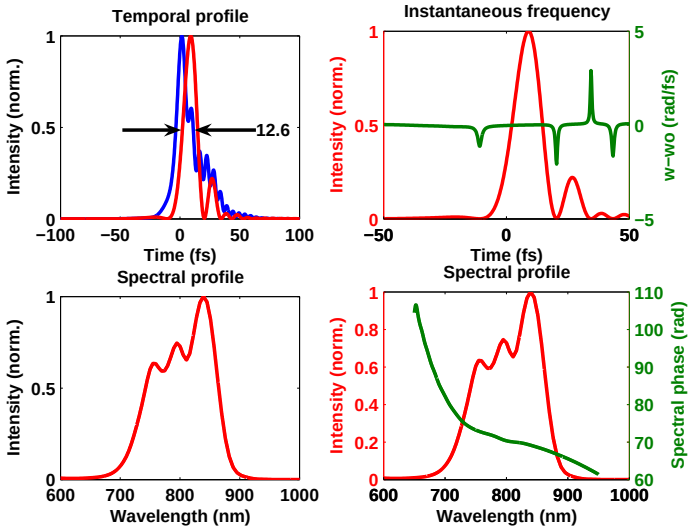

Figure 3.4: Temporal and spectral profiles of the pulse before (blue) and after (red) the exit window of the gas cell.

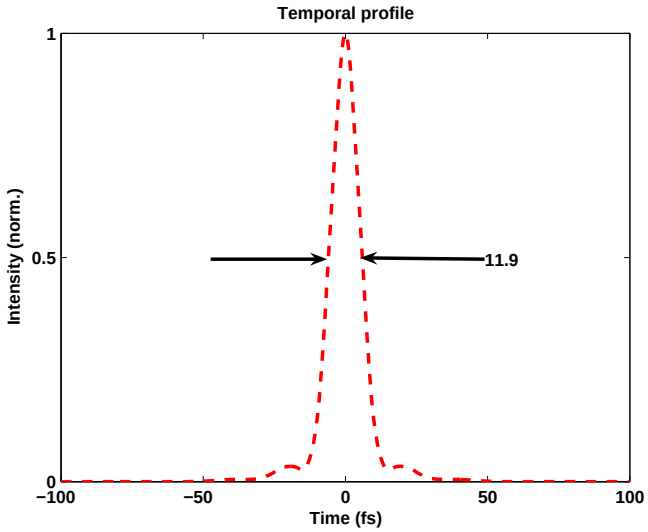

Figure 3.5: Transform limited output pulse.

3.4.2 Spatio-temporal coupling

Although the simulations of this Thesis do not include any spatial effects, they can explain rather well what actually takes place in a filament in a real physical situation. It is thus the conclusions from the simulations that pulse self-shaping only is a result of different *temporal* effects. The resulting chirp of the pulse is the result of a balance between different contributions, which for a specific set of input parameters is governed by the intensity. The spatio-temporal coupling exists in the sense that the spatial variation determines *the amount* of temporal reshaping of the pulse. Just as the interplay between the optical Kerr-effect and the plasma diffraction determines the *spatial* evolution of the light, the temporal counterpart SPM together with nonlinear plasma effects and dispersion shape the pulse *temporally*. To achieve a self-shaped, unchirped pulse for a specific setup with a certain input energy and gas pressure, the light must be focused in such a way that the number of focusing/defocusing stages add exactly the right amount of the different effects. It is also of importance that the input pulse is short enough, to induce enough dispersion in the plasma.

Filamentation is a process with a rather complex parameter-dependence. Changing the input parameters and amount of focusing, a new physical situation arises, resulting in a different spatial variation in the filament, not easy to predict. Therefore, the simulations of this Thesis should only be used as an *explanation* of a specific physical situation and *not* as a *prediction* of the outcome of a certain experiment. For that purpose, a full three-dimensional code should be used.

No matter the spatial variation inside the filament, self-shaping will always be present. However not necessarily with the right amount to achieve a near transform limited output pulse. If the correct spatial variation, i.e. one that induces exactly the right amount of SPM, nonlinear plasma effects and dispersion to the pulse, can not be achieved, the output pulse will have a chirp that has to be corrected for. If the chirp is negative, the pulse can be made to pass through a normal dispersive material (inducing a positive chirp), for example a piece of glass. If, on the other hand, the resulting chirp is positive, the light is made to impinge on a number of chirped mirrors, reducing the positive chirp. Chirped mirrors are further described in section 4.3.1. In the experimental part of this Thesis, a combination of the two solutions was used in order to achieve an exact balance between positive and negative chirp.

Chapter 4

Experiment

4.1 Setup

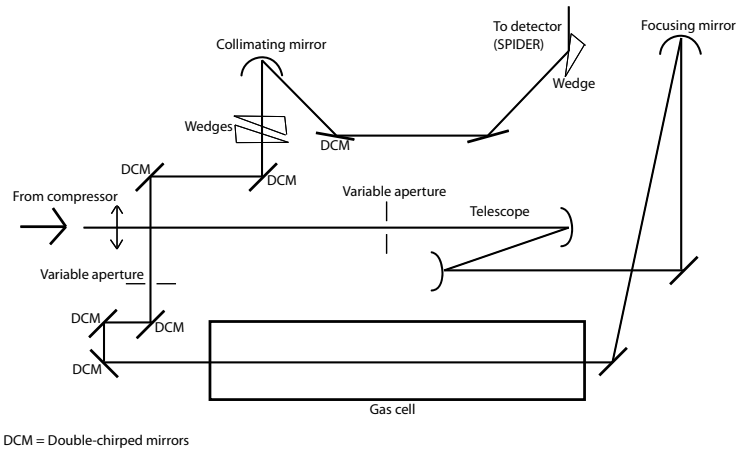

Figure 4.1: Schematic overview of the setup used in this Thesis.

4.2 The laser system

The experimental work of this Master Thesis has been performed at the Lund High-Power Laser Facility, with a 1 kHz-repetition rate, Ti:sapphire CPA-based laser system. The specifications of the system are:

Table 5.1 *The specifications of the kHz laser*

Oscillator output	5 nJ@76 MHz
Beam diameter $(1/e^2)$	8 mm (variable)
Pulse duration	35 fs
Pulse energy	2.5 mJ@1 kHz
Spectral bandwidth	∼35 nm

The system consists of the following parts:

1. **The oscillator**
   This device is based on Kerr-lens mode-locking in a Ti:sapphire crystal. In the oscillator, the dispersion is controlled with a set of prisms. To be able to precisely tune the temporal characteristics of the laser pulses, an acousto-optical programmable dispersive light modulator (AOPDF) is used, also known as a Dazzler [48]-[50]. This device shapes the pulses both spectrally and temporally before the amplification process starts. The reason in doing so is to try to counteract processes in the following chain of components, that will affect the final temporal output profile in a negative way. The output from the oscillator is first temporally stretched, using a grating-based device that introduces a positive chirp in the pulse, and is then sent into the first amplification step; the regenerative amplifier, also referred to as the regen. To couple the pulses from the oscillator into the regen, a Pockels cell is used that changes the polarisation of a few pulses, hereby making it possible for them to leave the oscillator.

2. **The regenerative amplifier (regen)**
   The regenerative amplifier is nothing but a common oscillator, with a Ti:sapphire crystal as the active medium. The pumping is provided by a Nd:YLF laser, at a repetition rate of 1 kHz. On its own the regen would produce pulses of only ns duration, but since it is seeded with the output from the oscillator before self-lasing starts, it will instead act as an effective amplifier. The pulses are left to bounce back and forth in the cavity, thus extracting all the available energy from the active medium. The polarisation is then changed once more by a second Pockels cell and the pulses are coupled out. Compared to the oscillator output, the pulses are amplified but still stretched in time, enabling further amplification.

3. **Further amplification**
   To achieve further amplification, the pulses are now made to pass through two more amplification steps (two- and multipass respectively), each with a Ti:sapphire crystal. Just as the regen, these amplification steps are pumped by a Nd:YLF laser at the repetition rate of 1 kHz.

4. **The compressor**
   The pulses have now been amplified to the maximum extent of the system

and should therefore be temporally recompressed before usage. This is accomplished with a compressor, consisting of two parallel gratings. By varying the angle of the gratings and their relative distance, compensation for the dispersion introduced by the stretcher and the amplification process in general is provided.

The pulses leaving the compressor should be of the same duration as before entering the amplification section. The only difference being an increased amount of energy. However, to be able to re-create the same pulse duration as before, the spectral bandwidth of the pulses must be preserved during the different amplification stages. One factor counteracting this requirement is *gain narrowing* in the amplification process; arising since the central frequencies of the spectrum (containing most of the pulse energy) extract the most gain from the medium. This results in a narrowing of the spectrum. By reducing the power density in the central part of the pulse, before or during the amplification, more energy will be left to amplify the wings, resulting in amplified pulses with a broader spectrum than before. In the kHz laser, the AOPDF is used to reduce the gain narrowing [51].

4.3 Optics

In this section, the different optical components used in the setup will be described, as well as their function.

1. **Apertures**
   Two apertures of variable size are placed before and after the gas cell. The first aperture enables variation of the input energy, while the second makes it possible to vary the transverse extent of the filament used for compression.

2. **Telescope**
   This device consists of two silver coated mirrors, the first being concave and the second convex, with a radius of curvature of 1 m and 0.50 m respectively. By varying the separation between the two mirrors, the radius of the beam at the focusing mirror changes, hence affecting the size of the focus in the gas cell. In this way, a smooth variation of the input intensity is possible.

3. **Focusing mirror**
   Consists of a silver coated, concave mirror with a radius of curvature of 2.0 m. The mirror focuses the laser light in the gas, initiating filamentation. Depending on the mirror separation in the telescope, the location and size of the focus varies.

4. **Chirped mirrors**
   The setup includes six double-chirped mirrors, each inducing a negative dispersion of approximately -50 fs^2 in the reflected pulse.

5. **Collimating mirror**
   A silver coated, concave mirror collimates the reflected light from the chirped mirrors.

6. **Wedges**
   One wedge reflects the collimated light into the detector, see section 4.4. Two other wedges are used to induce a variable amount of positive dispersion in the setup, enabling an exact balance of the contribution from the chirped mirrors.

7. **Totally reflecting mirrors**
   In the setup a number of totally reflecting mirrors are also used, only changing the direction of the beam.

4.3.1 Chirped mirrors

Chirped mirrors consist of multiple dielectric layers of varying thickness. According to the Bragg equation

$$m\lambda = 2d\sin\theta \tag{4.1}$$

different frequencies will be reflected at different depths, introducing a group-delay dispersion (GDD), $\frac{d^2\varphi(\omega)}{d\omega^2}$, in the pulse. In equation (4.1), d denotes the separation of the different layers and θ the angle of incidence [52]. If the chirp of a pulse is known, a reflecting layer structure can be created in a way that makes the different frequency components exit at the same time, i.e. a chirp-free pulse can be created. However, only a linear frequency modulation can be compensated for in this way.

To obtain high reflectivity and low absorption, layer pairs with alternating high and low refractive indices are used, for instance TiO_2 (n $\approx$ 2.4) and SiO_2 (n $\approx$ 1.45). Depending on the layer structure, a number of different types of chirped mirrors exist. By using quarter-wave layer pairs of increasing thickness, the Bragg wavelength increases linearly in the structure, reflecting high frequencies at the surface and lower frequencies at larger depths. The chirped mirror hence induces a negative GDD in the pulse. This type of mirror is commonly referred to as simple-chirped [53].

Since the induced group-delay neither varies linearly nor smoothly with wavelength, the induced dispersion properties of simple-chirped mirrors are inadequate for generation of ultrashort laser pulses [54]. A mirror that however can provide ultrashort pulses is the double-chirped mirror (DCM). The main difference between simple- and double-chirped mirrors is the addition of an anti-reflection coating in the latter, as well as an impedance-matching layer at the front of the mirror. The anti-reflection coating matches the mirror to the surrounding air and works over a broadband region [53][55].

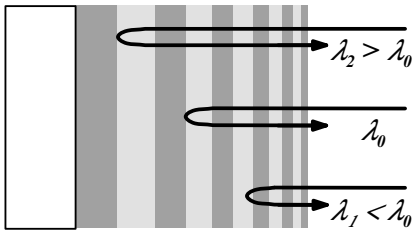

Figure 4.2: Schematic picture of the general layer structure of chirped mirrors [56].

4.4 Spectral phase interferometry for direct electric-field reconstruction

To be able to measure an optical light pulse correctly, the response time of the detector has to be comparable to the pulse duration. This causes problems for ultrashort pulses, since the response times of the detectors available today are many orders of magnitude too long. Therefore, alternative methods have to be used. One method is SPIDER, an acronym for *spectral phase interferometry for direct electric-field reconstruction*, which has been used to characterise the electric field of the compressed pulses in this Thesis [57].

In spectral interferometry in general, the spectral phase is reconstructed by calculating the phase difference, $\Delta\varphi(\omega)$, between two pulses that are made to propagate different optical paths in the two arms of an interferometer. The interferometer is based upon amplitude-division, which means that the initial pulse is divided into two parts by some kind of beam splitter. Depending on the value of $\Delta\varphi(\omega)$, the electric fields of the two pulses will either interfere constructively or destructively at recombination. The resulting *interferogram* is resolved by a spectrometer and can be written as:

$$\begin{aligned} I(\omega) &= |E_0(\omega) + E(\omega)\exp(i\omega\tau)|^2 = \\ &= |E_0(\omega)|^2 + |E(\omega)|^2 + [E_0^*(\omega)E(\omega) \times \exp(i\omega\tau) + c.c.] \end{aligned} \quad (4.2)$$

where $E_0(\omega)$ and $E(\omega)$ denote the Fourier transform of the two replicas and τ represents their relative time delay (controlled by the difference in optical path length in the interferometer). By retrieving $\Delta\varphi(\omega) = \arg[E(\omega)] - \arg[E_0(\omega)]$ from the interferogram, the spectral phase of the pulse can be reconstructed and hence the temporal duration determined, see further [58].

The SPIDER reconstruction of the spectral phase includes some additional aspects compared to the general method of spectral interferometry. Here the two replicas have a relative temporal delay τ, as well as a spectral shear Ω. The spectral shear is obtained by upconverting the two replicas with different parts of a chirped pulse in a nonlinear crystal. Since both τ and Ω are fixed, the interferogram is described by:

$$\begin{aligned} D(\omega) &= |E(\omega-\Omega)|^2 + |E(\omega)|^2 + \\ &+ 2|E(\omega-\Omega)E(\omega)|\cos[\varphi(\omega-\Omega) - \varphi(\omega) - \tau\omega] \end{aligned} \quad (4.3)$$

with a nominal fringe spacing of $\frac{2\pi}{\tau}$. The phase difference, $\varphi(\omega-\Omega) - \varphi(\omega)$, between two frequency components in the input pulse causes a perturbation of the fringes, which is used to reconstruct the spectral phase.

The interferogram can be written as a sum of three different parts, where two of them contain information about the spectral phase. By Fourier transforming the interferogram into the time domain, the different contributions will be separated if the temporal delay between the two replicas is large enough. The term of interest is then chosen by multiplying the Fourier transformed interferogram with a filter function. As a last step an inverse Fourier transform back to the frequency domain is performed. For this purpose, an algorithm developed by Takeda *et al.* is often used [59]. The argument of the chosen interferogram can be expressed as:

$$\varphi(\omega) - \varphi(\omega-\Omega) + \tau\omega \quad (4.4)$$

To be able to remove the linear phase term $\tau\omega$ from equation (4.4), information about this quantity is required. This is provided by recording a reference interferogram for the two relatively temporally delayed pulses, without any spectral shear imparted. Since the interfering pulses now are identical, the only contributing phase difference is due to the temporal delay, $\tau\omega$.

When the linear phase term has been removed, the spectral phase can be reconstructed from the phase difference. The following expression is used:

$$\theta(\omega) \equiv \varphi(\omega) - \varphi(\omega - \Omega) \tag{4.5}$$

To reconstruct $\varphi(\omega)$ from $\theta(\omega)$ concatenation is used, which returns a sampled spectral phase at intervals of Ω across the spectrum. Since the phase is created out of relative phase differences, the spectral phase at some arbitrary frequency is set to zero, for instance ω_0, so that $\varphi(\omega_0 - \Omega) = -\theta(\omega_0)$. According to the Whittaker-Shannon sampling theorem [60], it is then enough just to add up these phase differences to reconstruct the spectral phase. If the spectral shear can be considered as small relative to the structure of the spectral phase, the phase difference is approximately described by the first derivative of the spectral phase, i.e.

$$\theta(\omega) \equiv \varphi(\omega) - \varphi(\omega - \Omega) \approx \Omega \frac{d\varphi(\omega)}{d\omega} \tag{4.6}$$

From this expression, the spectral phase can finally be constructed by integration [57]

$$\varphi(\omega) \approx \frac{1}{\Omega} \int \theta(\omega)\, d\omega \tag{4.7}$$

The SPIDER setup used in this Thesis is schematically depicted in figure 4.3. In order to measure the pulses correctly, the full bandwidth must be maintained

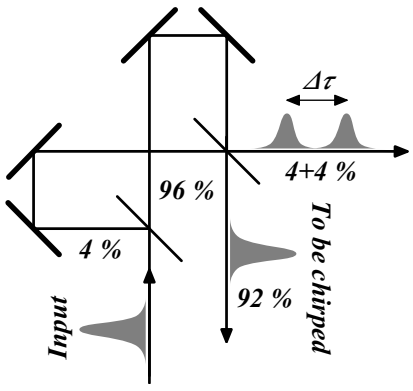

Figure 4.3: Schematic picture of the SPIDER setup in Lund [61].

throughout the setup. The optical components that can limit the bandwidth are the mirrors, the nonlinear crystal and the beam splitters. If silver mirrors and a thin type II BBO crystal are used, a very broad bandwidth will be reflected and upconverted. Concerning the beam splitters, they must be very thin in order not to stretch the short pulse replicas. By using two thin windows, a

broadband reflectivity is guaranteed, producing two pulses with little energy and one pulse with more energy. Using this design, the incoming pulse enters the first beam splitter, where only 4% is reflected and is led to one of the interferometer arms with an adjustable delay stage. The remaining 96% is transmitted and enters the other arm. The two relatively temporally delayed replicas then reach the second beam splitter, where the 4%-pulse is transmitted, since this side of the beam splitter is anti-reflection coated. Of the 96%-pulse, 4% is reflected and 92% is transmitted to a piece of glass, where it gets stretched and thus chirped. To make sure that the two 4%-replicas become spectrally sheared, the stretched pulse must be centred on them. The 92%-pulse therefore enters another adjustable delay stage and finally recombines with the two replicas in a frequency doubling BBO crystal. If the two replicas and the stretched pulse spatially overlap, a SPIDER interferogram can be generated [62].

4.5 Results and discussion

Since filamentation is a process with a complex parameter-dependence, it was of interest to study this experimentally. The information gained was then used to try to optimise the technique. Three different measurement series were performed and the outcome can be found in the sections below. In section 4.5.1, the influence of the gas pressure in the cell is studied. In section 4.5.2, the diameter of the aperture prior to the gas cell is varied, thereby varying the input energy as well as the size of the geometrical focus. Finally in section 4.5.3, different mirror separations in the telescope are used, changing the size of the geometrical focus. In all the measurements, the temporal and spectral characterisations of the output pulses were performed with the SPIDER.

4.5.1 Pressure

To figure out which effect a varying pressure had on the output pulse, a number of different pressures between 600 and 1200 mbar were used. The input energy was 1.4 mJ (from the compressor) and the variable aperture before the gas cell had a diameter of about 10 mm, to spatially filter the beam sent into the gas cell. The result is seen in figure 4.4. The input intensity used should be about $6 \cdot 10^{13}$ W/cm^2, according to calculations. As is seen in the figure, the

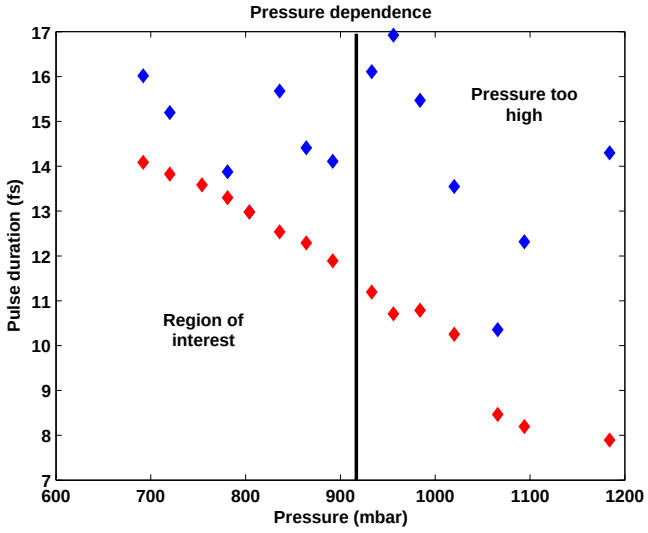

Figure 4.4: Output pulse duration (blue) as a function of the pressure in the gas cell. Shown are also the transform limited pulses (red). The input energy is 1.4 mJ and the diameter of the aperture before the gas cell is 10 mm.

transform limited pulses show a clear trend: the higher the pressure, the shorter the pulses. This has to do with the fact that a higher pressure provides a higher number of atoms and hence a larger spectral broadening, see figure 4.5. This trend is however only true up to a certain pressure, beyond which the spatial beam profile is destroyed. This occurs in the region above 900 mbar. The compressed pulses also seem to follow this trend, however not as clear as the

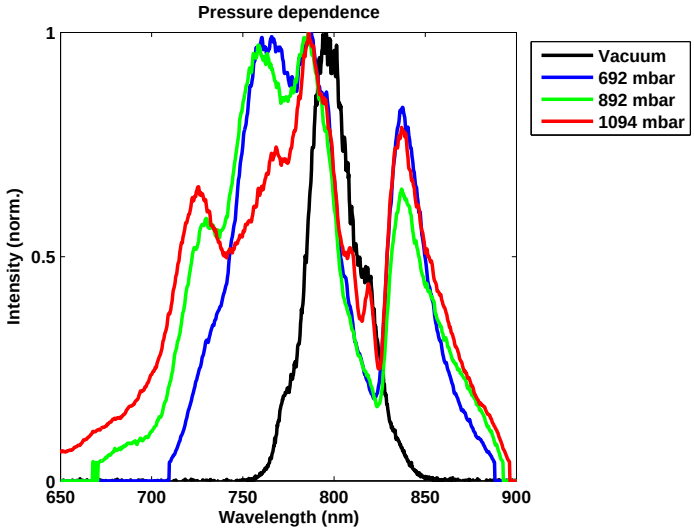

Figure 4.5: Output spectrum as a function of the pressure in the gas cell.

transform limited counterpart. This probably has to do with the fact that a certain input intensity only can ionise a certain number of atoms, in that sense controlling the balance between SPM and plasma effects. If the pressure is too high, the contributions from the different effects will be unfavourable from a pulse self-shaping point of view and beyond external correction by the chirped mirrors.

Since maximising the output energy also was of interest in this Thesis, this parameter was measured for each pressure. The region of interest is marked in figure 4.6. The output energy is thus rather constant over almost the entire pressure region. The reason for this is probably that the input intensity is constant, determining the balance between SPM and plasma effects, affecting the light guiding properties inside the filament.

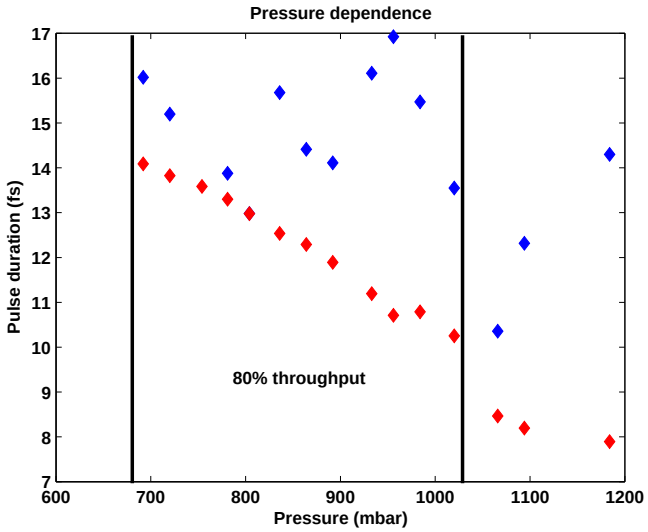

Figure 4.6: Energy throughput for different pressures in the gas cell.

4.5.2 Aperture

For further optimisation a constant pressure was used, while the diameter of the aperture prior to the cell was varied. In this way both the input energy as well as the size of the focus were affected, i.e. the input intensity was changed. The result can be seen in figure 4.7, together with the energy throughput. A pressure of 959 mbar was used. Compared to the pressure measurements, it is

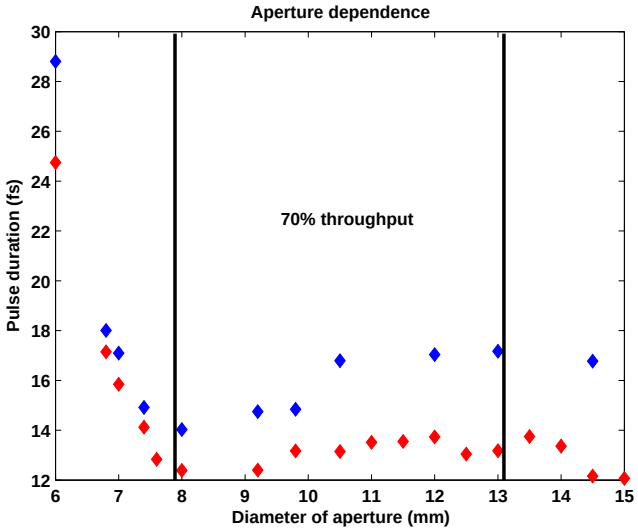

Figure 4.7: Output pulse duration (blue) as a function of the size of the aperture before the gas cell. Shown are also the transform limited pulses (red). The region with optimum energy throughput is marked. The pressure in the cell is 959 mbar.

hard to draw any real conclusions here. Each aperture results in a different input intensity, creating a new spatial variation. In other words, another physical situation arises [63]. However, it seems like there exists a minimum, supporting the theory that the shortest pulse is obtained when an exact balance between SPM and plasma effects is met. In the present case corresponding to an aperture of 8.0 mm diameter.

4.5.3 Telescope

As a final test, a few different mirror separations in the telescope were used. By varying the mirror separation, the radius of the beam is changed as well as the position and size of the focal spot. Even the smallest change has a large effect and in order not to risk damaging any optical components by moving the focus too much, the number of measurement points were reduced. The result is clear and can be seen in figure 4.8. One mirror separation of 27.5 cm results in the required balance of SPM and plasma contributions to produce the shortest pulse. The pressure in the cell is 977 mbar and the diameter of the aperture is 8.0 mm. Thus the highest amount of focusing does not produce the shortest

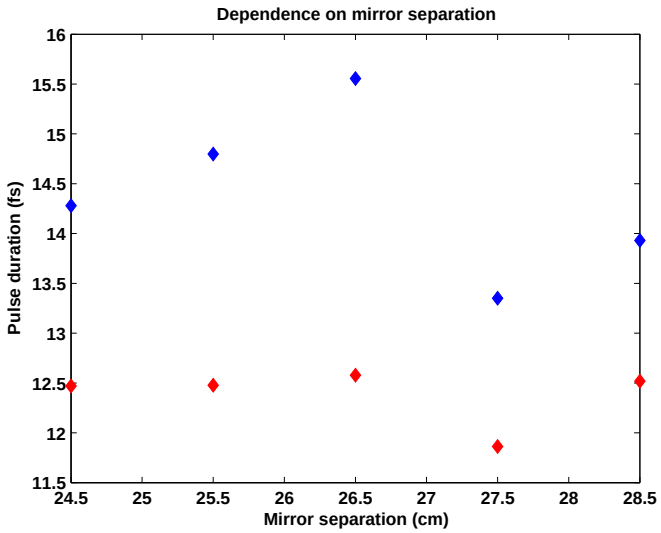

Figure 4.8: Output pulse duration (blue) as a function of the mirror separation in the telescope before the gas cell. Shown are also the transform limited pulses (red). The pressure in the gas cell is 977 mbar and the diameter of the aperture is 8.0 mm.

pulse. The reason for this is seen in figure 4.9. A high degree of ionisation limits the number of neutral atoms, responsible for the broadening.

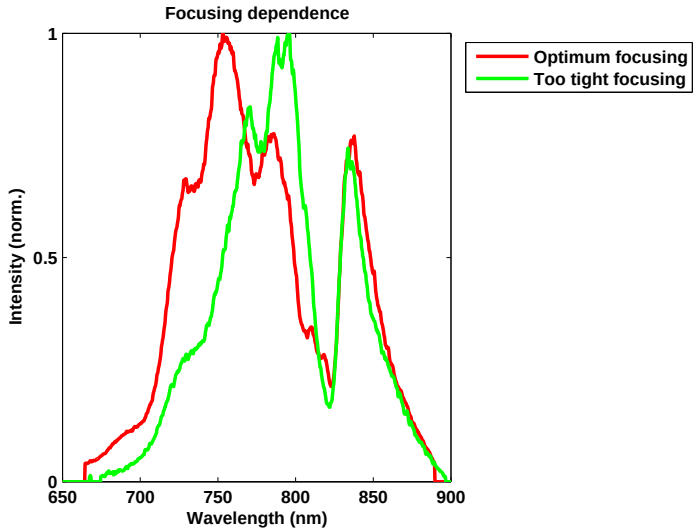

Figure 4.9: Output spectrum as a function of the amount of focusing.

4.5.4 Best result

After having varied the parameters in three independent measurement series, it was found that the following set provided the best result: a pressure of 977 mbar in the cell, an aperture of 8.0 mm diameter prior to the gas cell and a spacing of 27.5 cm between the mirrors in the telescope. The resulting temporal and spectral profiles of the output are found in figures 4.10 and 4.11.

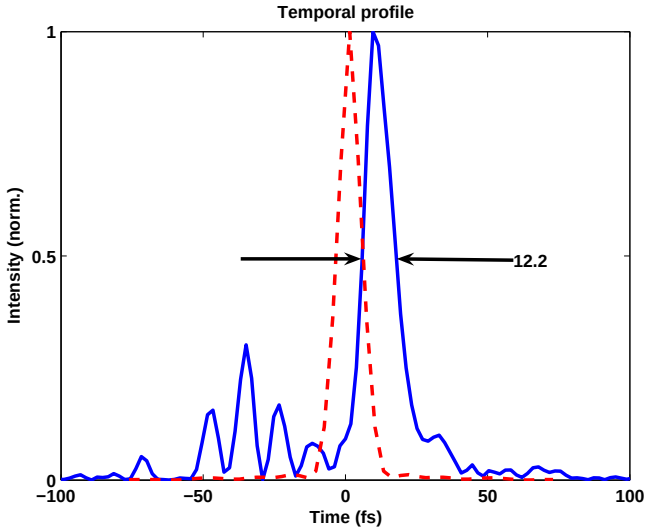

Figure 4.10: Temporal profile of the output pulse (blue) for the optimised setup of this Thesis, together with the transform limited pulse (dashed red). The pressure in the cell is 977 mbar, the diameter of the aperture is 8.0 mm and the mirror separation in the telescope is 27.5 cm. The duration of the transform limited pulse is 10.3 fs.

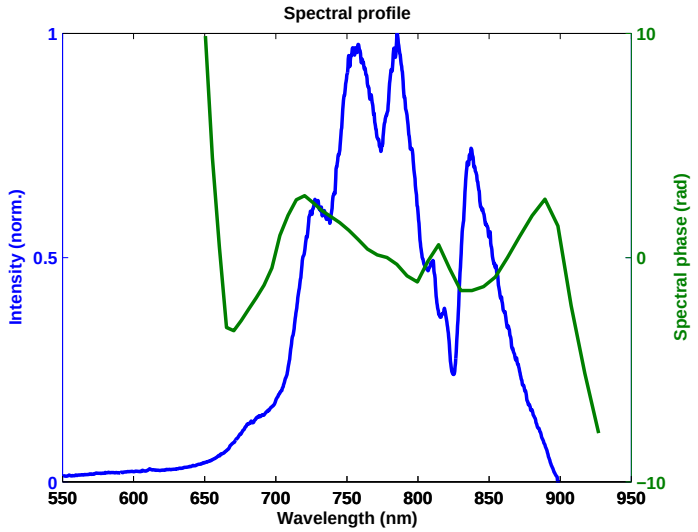

Figure 4.11: Output spectrum, together with the spectral phase, for the optimised setup of this Thesis. The pressure in the cell is 977 mbar, the diameter of the aperture is 8.0 mm and the mirror separation in the telescope is 27.5 cm.

Chapter 5

Conclusion and outlook

In this Master Thesis, the temporal aspects of the filamentation pulse compression technique have been studied. The work has included both theory and experiment. Theoretically, self-shaping of the pulse has been confirmed and explained. Also, the somewhat complex spatio-temporal coupling has been briefly touched upon. It is the general belief of this Thesis that it only exists in the sense that the spatial variations determine the amount of different temporal effects induced in the pulse. Experimentally, the parameter dependence of filamentation has been studied in trying to optimise the technique. The best result was a pulse with a duration of 12.2 fs (10.3 fs transform limited).

The work of this Thesis has been performed in the research group of "Attosecond Physics & High-Order Harmonic Generation" at Lund Institute of Technology. High-order harmonic generation in gases has stimulated a lot of research activity due to its ability to create short pulse, coherent radiation in the XUV and soft X-ray wavelength region. By adding several high-order harmonics, a broad spectral bandwidth can be obtained, enabling the generation of pulses with a duration in the attosecond region (1 as = 10^{-18} s). This field of science is hence called *attophysics* [64].

Filamentation is interesting for harmonic generation research in several aspects. If the output energy is high, the technique can be used to generate short pulse harmonics with a high efficiency. This will also be interesting for the production of single attosecond pulses, so far obtained by using 5 fs laser pulses [65].

Another idea is to generate harmonics directly in the filament. It has recently been verified that the third harmonic generated in air during filamentation by an IR femtosecond laser pulse has a conversion efficiency as high as 0.2% [66]. Another example is the third and fifth harmonic generated in an UV-filament in argon, which show a conversion efficiency of 0.02% and 0.01% respectively, corresponding to at least two orders of magnitude higher than without filamentation [67]. This has to do with the fact that filamentation provides a light pulse with nearly constant high intensity and flat phase front, which helps phase matching. Recently, high-order harmonics have been efficiently produced in a small filament in Lund [68].

Bibliography

[1] Orazio Svelto. *Principles of Lasers, Fourth Edition,* page 331. Plenum Press, New York (1998).

[2] Jean-Claude Diels, Wolfgang Rudolph. *Ultrashort laser pulse phenomena,* page 9. Academic Press, San Diego (1996).

[3] Orazio Svelto. *Principles of Lasers, Fourth Edition,* page 334. Plenum Press, New York (1998).

[4] Orazio Svelto. *Principles of Lasers, Fourth Edition,* page 344-345. Plenum Press, New York (1998).

[5] Sune Svanberg. *Atomic and Molecular Spectroscopy, Basic Aspects and Practical Applications, Fourth Edition,* pages 282-283. Springer-Verlag, Berlin Heidelberg (2004).

[6] Johan Mauritsson. *Temporal Aspects of High-Intensity Laser-Matter Interactions,* page 26. Department of Physics, Lund Institute of Technology (2003).

[7] Orazio Svelto. *Principles of Lasers, Fourth Edition,* page 345. Plenum Press, New York (1998).

[8] W.J. Tomlinson, R.H. Stolen and C.V. Shank. *Compression of optical pulses chirped by self-phase modulation in fibers,* J. Opt. Soc. Am. B **1(2)**:139-149 (1984).

[9] M. Nisoli, S. De Silvestri and O. Svelto. *Generation of high energy 10 fs pulses by a new pulse compression technique,* Appl. Phys. Lett. **68(20)**:2793-2795 (1996).

[10] C.P. Hauri, W. Kornelis, F.W. Helbing, A. Heinrich, A. Couairon, A. Mysyrowicz, J. Biegert, U. Keller. *Generation of intense, carrier-envelope phase-locked few-cycle laser pulses through filamentation,* Appl. Phys. B (2004).

[11] C.P. Hauri, A. Guandalini, P. Eckle, W. Kornelis, J. Biegert, U. Keller. *Generation of intense few-cycle laser pulses through filamentation - parameter dependence,* Optics Express, vol. 13, no. 19 (19 September 2005).

[12] A. Braun, G. Korn, X. Liu, D. Du, J. Squier and G. Mourou. Opt. Lett. **20**:73 (1995).

[13] A. Couairon, S. Tzortzakis, L. Bergé, M. Franco, B. Prade and A. Mysyrowicz. *Infrared femtosecond light filaments in air: simulations and experiments,* J. Opt. Soc. Am. B., vol. 19, no. 5 (May 2002).

[14] Frank L. Pedrotti S.J., Leno S. Pedrotti. *Introduction to optics,* page 2. Prentice-Hall Inc., Upper Saddle River, New Jersey.

[15] Jean-Claude Diels, Wolfgang Rudolph. *Ultrashort laser pulse phenomena,* page 6. Academic Press, San Diego (1996).

[16] Johan Mauritsson. *Temporal Aspects of High-Intensity Laser-Matter Interactions,* pages 11-12. Department of Physics, Lund Institute of Technology (2003).

[17] Johan Mauritsson. *Temporal Aspects of High-Intensity Laser-Matter Interactions,* page 12. Department of Physics, Lund Institute of Technology (2003).

[18] Govind P.Agrawal. *Nonlinear fiber optics, Third Edition,* page 68. Academic Press, San Diego (2001).

[19] Johan Mauritsson. *Temporal Aspects of High-Intensity Laser-Matter Interactions,* pages 12-13. Department of Physics, Lund Institute of Technology (2003).

[20] Govind P. Agrawal. *Nonlinear fiber optics, Third Edition,* page 9. Academic Press, San Diego (2001).

[21] Govind P. Agrawal. *Nonlinear fiber optics, Third Edition,* page 12. Academic Press, San Diego (2001).

[22] Govind P. Agrawal. *Nonlinear fiber optics, Third Edition,* pages 77-78. Academic Press, San Diego (2001).

[23] Govind P. Agrawal. *Nonlinear fiber optics, Third Edition,* page 18. Academic Press, San Diego (2001).

[24] Govind P. Agrawal. *Nonlinear fiber optics, Third Edition,* page 99. Academic Press, San Diego (2001).

[25] L.A. Ostrovskii. Sov. Phys. JETP **24**:797 (1967).

[26] R.J. Jonek and R. Landauer. Phys. Lett. **24A**:228 (1967).

[27] F. DeMartini, C.H. Townes, T.K. Gustafson and P.L. Kelley. Phys. Rev. **164**:312 (1967).

[28] D. Grischkowsky, E. Courtens and J.A. Armstrong. Phys. Rev. Lett. **31**:422 (1973).

[29] R.L. Fork, C.V. Shank, C. Herlimann, R. Yen and W.J. Tomlinson. Opt. Lett. **8**:1 (1983).

[30] G. Yang and Y.R. Shen. Opt. Lett. **9**:510 (1984).

[31] J.T. Manassah, M.A. Mustafa, R.R. Alfano and P.P. Ho. Phys. Lett. **113A**:242 (1985); IEEE J. Quantum Electron. **22**:197 (1986).

[32] D. Mestdagh and M. Haelterman. Opt. Commun. **61**:291 (1987).

[33] B.R. Suydam, R.R. Alfano ed., *Supercontinuum Laser Source,* chapter 6. Springer-Verlag, New York (1989).

[34] F.A. Ilkov, J.E. Decker and S.L. Chin. *Ionization of atoms in the tunneling regime with experimental evidence using Hg atoms,* J. Phys. B:At. Mol. Opt. Phys **25**:4005-4020 (1992).

[35] Johan Mauritsson. *Temporal Aspects of High-Intensity Laser-Matter Interactions,* page 36. Department of Physics, Lund Institute of Technology (2003).

[36] Johan Mauritsson. *Temporal Aspects of High-Intensity Laser-Matter Interactions,* pages 9-10. Department of Physics, Lund Institute of Technology (2003).

[37] A. Chiron, B. Lamouroux, R. Lange, J.-F. Ripoche, M. Franco, B. Prade, G. Bonnaud, G. Riazuelo and A. Mysyrowicz. *Numerical simulations of the nonlinear propagation of femtosecond optical pulses in gases,* Eur. Phys. J. D **6**:383-396 (1999).

[38] M.V. Ammosov, N.B. Delone and V.P. Kraĭnov. *Tunnel ionization of complex atoms and of atomic ions in an alternating electromagnetic field,* Zh. Eksp. Teor. Fiz. **91**:2008-2013 (December 1986).

[39] Govind P. Agrawal. *Nonlinear fiber optics, Third Edition* page 64. Academic Press, San Diego (2001).

[40] Govind P. Agrawal. *Nonlinear fiber optics, Third Edition* pages 122-123. Academic Press, San Diego (2001).

[41] T.R. Taha and M.J. Ablowitz. J. Comput. Phys. **55**:203 (1984).

[42] R.H. Hardin and F.D. Tappert. SIAM Rev. Chronicle **15**:423 (1973).

[43] R.A. Fisher and W.K. Bischel. Appl. Phys. Lett. **23**:661 (1973); J. Appl. Phys. **46**:4921 (1975).

[44] Govind P. Agrawal. *Nonlinear fiber optics, Third Edition,* pages 51-52. Academic Press, San Diego (2001).

[45] Johan Mauritsson. *Pulse Propagation Through Different Materials User-Friendly Simulation Software,* Lund Reports on Atomic Physics LRAP-310, Lund (August 2000).

[46] Govind P. Agrawal. *Nonlinear fiber optics,* page 43. Academic Press, San Diego (1989).

[47] C.P. Hauri *et al.*, to be published.

[48] P. Tournois. *Acousto-optic programmable dispersive filter for adaptive compensation of group delay time dispersion in laser systems,* Opt. Commun. **140**:245 (1997).

[49] F. Verluise, V. Laude, Z. Cheng, Ch. Spielmann and P. Tournois. *Amplitude and phase control of ultrashort pulses by use of an acousto-optic programmable dispersive filter: pulse compression and shaping,* Opt. Lett. **25**:575 (2000).

[50] D. Kaplan and P. Tournois. *Theory and performance of the acousto-optic programmable dispersive filter used for femtosecond pulse shaping,* J. Phys. IV France, **12**:69 (2002).

[51] Johan Mauritsson. *Temporal Aspects of High-Intensity Laser-Matter Interactions,* pages 27-30. Department of Physics, Lund Institute of Technology (2003).

[52] Frank L. Pedrotti S.J., Leno S. Pedrotti. *Introduction to optics,* page 274. Prentice-Hall Inc., Upper Saddle River, New Jersey.

[53] Nicolai Matuschek, Franz X. Kärtner and Ursula Keller. *Theory of Double-Chirped Mirrors,* IEEE Journal of selected topics in quantum electronics, vol. 4, no. 2 (March/April 1998).

[54] P. Laporta and V. Magni. *Dispersive effects in the reflection of femtosecond optical pulses from broadband dielectric mirrors,* Appl. Opt., vol. 24, pages 2014-2020 (1985).

[55] N. Matuschek, L. Gallman, D.H. Sutter, G. Steinmeyer, U. Keller. *Back-side-coated chirped mirrors with ultra-smooth broadband dispersion characteristics,* Appl. Phys. B **71**:509-522 (2000).

[56] Johan Mauritsson. *Temporal Aspects of High-Intensity Laser-Matter Interactions,* page 31. Department of Physics, Lund Institute of Technology (2003).

[57] C. Iaconis and I.A. Walmsley. *Self-Referencing Spectral Interferometry for Measuring Ultrashort Optical Pulses,* IEEE Journal of Quantum Electronics, vol. 35, no. 4 (April 1999).

[58] Christophe Dorrer, Nadia Belabas, Jean-Pierre Likforman and Manuel Joffre. *Spectral resolution and sampling issues in Fourier-transform spectral interferometry,* J. Opt. Soc. Am. B, vol. 17, no. 10 (October 2000).

[59] M. Takeda, H. Ina and S. Kobayashi. *Fourier-transform method of fringe-pattern analysis for computer-based topography and interferometry,* J. Opt. Soc. Amer., vol. 72, page 156 (1982).

[60] J.W. Goodman. *Introduction to Fourier Optics,* New York: McGraw-Hill, chapter 2 (1988).

[61] Johan Mauritsson. *Temporal Aspects of High-Intensity Laser-Matter Interactions,* page 24. Department of Physics, Lund Institute of Technology (2003).

[62] Johan Mauritsson. *Temporal Aspects of High-Intensity Laser-Matter Interactions,* pages 23-24. Department of Physics, Lund Institute of Technology (2003).

[63] Discussion with C.P. Hauri, Laboratoire d'Optique Appliquée.

[64] Johan Mauritsson. *Temporal Aspects of High-Intensity Laser-Matter Interactions,* pages 6-7. Department of Physics, Lund Institute of Technology (2003).

[65] R. Kienberger, E. Goulielmakis, M. Uiberacker, A. Baltuska, V. Yakovlev, F. Bammer, A. Scrinzi, Th. Westerwalbesloh, U. Kleineberg, U. Heinzmann, M. Drescher and F. Krausz. *Atomic transient recorder,* Nature **427**:817-821 (2004).

[66] F. Théberge, N. Aközbek, W. Liu, J.-F. Gravel, S.L. Chin. *Third harmonic beam profile generated in atmospheric air using femtosecond laser pulses,* Optics Communications **245**:399-405 (2005).

[67] N. Kortsalioudakis, M. Tatarakis, N. Vakakis, S.D. Moustaizis, M. Franco, B. Prade, A. Mysyrowicz, N.A. Papadogiannis, A. Couairon, S. Tzortzakis. *Enhanced harmonic conversion efficiency in the self-guided propagation of femtosecond ultraviolet laser pulses in argon,* Appl. Phys. B **80**:211-214 (2005).

[68] T. Ruchon *et al.*, in preparation.

[69] Govind P. Agrawal. *Nonlinear fiber optics, Third Edition,* pages 31-32. Academic Press, San Diego (2001).

[70] Govind P. Agrawal. *Nonlinear fiber optics, Third Edition,* pages 39-40. Academic Press, San Diego (2001).

[71] Govind P. Agrawal. *Nonlinear fiber optics, Third Edition* pages 43-44. Academic Press, San Diego (2001).

[72] F.M. Mitschke and L.F. Mollenauer. Opt. Lett. **11**:659 (1986).

[73] J.P. Gordon. Opt. Lett. **11**:662 (1986).

[74] Y. Kodama and A. Hasegawa. IEEE J. Quantum Electron. **23**:510 (1987).

[75] E.A. Golovchenko, E.M. Dianov, A.N. Pilipetskii, A.M. Prokhorov and V.N. Serkin. Sov. Phys. JETP. Lett. **45**:91 (1987).

[76] R.H. Stolen, J.P. Gordon, W.J. Tomlinson and H.A. Haus. J. Opt. Soc. Am. B. **6**:1159 (1989).

[77] K.J. Blow and D. Wood. IEEE J. Quantum Electron. **25**:2665 (1989).

[78] P.V. Mamyshev and S.V. Chernikov. Opt. Lett. **15**:1076 (1990).

[79] S.V. Chernikov and P.V. Mamyshev. J. Opt. Soc. Am. B **8**:1633 (1991).

[80] P.V. Mamyshev and S.V. Chernikov. Sov. Lightwave Commun. **2**:97 (1992).

[81] R.H. Stolen and W.J. Tomlinson. J. Opt. Soc. Am. B **9**:565 (1992).

[82] S. Blair and K. Wagner. Opt. Quantum Electron. **30**:697 (1998).

[83] Govind P. Agrawal. *Nonlinear fiber optics, Third Edition* page 49. Academic Press, San Diego (2001).

[84] Govind P. Agrawal. *Nonlinear fiber optics, Third Edition* page 44. Academic Press, San Diego (2001).

[85] B.H. Bransden and C.J. Joachin. *Physics of Atoms and Molecules, Second edition,* page 168. Pearson Education Limited (2003).

[86] B.H. Bransden and C.J. Joachin. *Physics of Atoms and Molecules, Second Edition,* pages 281-284. Pearson Education Limited (2003).

[87] *http://www.worldhistory.com/wiki/W/WKB-approximation.htm.*

[88] B.H. Bransden and C.J. Joachin. *Physics of Atoms and Molecules, Second Edition,* page 137. Pearson Education Limited (2003).

[89] B.H. Bransden and C.J. Joachin. *Physics of Atoms and Molecules, Second Edition,* page 286. Pearson Education Limited (2003).

[90] M.V. Ammosov, N.B. Delone and V.P. Kraĭnov. *Ionization dynamics in strong laser fields,* Sov. Phys. JETP **64**:1191 (1986).

[91] Elena Gubbini. *Multiple Ionization of Heavy Atoms in Super Strong Laser Fields,* Mathematik und Naturwissenschaften der Technischen Universität Berlin (2005).

[92] CVI Laser Corporation. *Laser Optics and Coatings* (1997).

[93] A. Dalgarno and A. E. Kingston. *The refractive indices and verdet constants of inert gases,* Proc. R. Soc. London **259**:424-429 (1966).

[94] J.-F. Ripoche. *Mesure Du Profil Temporel Exact D'impulsions Laser Femtosecondes Intenses,* PhD Thesis, l'École Polytechnique (1998).

[95] E.T.J. Nibbering, G. Grillon, M.A. Franco, B.S. Prade and A. Mysyrowicz. *Determination of the inertial contribution to the nonlinear refractive index of air, n-2 and o-2 by use of unfocused high-intensity femtosecond laser pulses,* J. Opt. Soc. Am. B **14(3)**:650-660 (1997).

Appendix A

The propagation equation

The propagation of light in media is governed by Maxwell's equations

$$\nabla \times \mathbf{E} = -\frac{\partial \mathbf{B}}{\partial t} \tag{A.1}$$

$$\nabla \times \mathbf{H} = \mathbf{J} + \frac{\partial \mathbf{D}}{\partial t} \tag{A.2}$$

$$\nabla \cdot \mathbf{D} = \rho_f \tag{A.3}$$

$$\nabla \cdot \mathbf{B} = 0 \tag{A.4}$$

where $\mathbf{E}$ and $\mathbf{H}$ represent the electric and magnetic field vectors, $\mathbf{D}$ and $\mathbf{B}$ the corresponding electric and magnetic flux densities and $\mathbf{J}$ and ρ_f the current and charge densities of the medium. The flux densities arise as a response of the medium interacting with the electromagnetic field and can be written as:

$$\mathbf{D} = \varepsilon_0 \mathbf{E} + \mathbf{P} \tag{A.5}$$

$$\mathbf{B} = \mu_0 \mathbf{H} + \mathbf{M} \tag{A.6}$$

where ε_0 and μ_0 are the vacuum permitivity and permeability respectively. $\mathbf{P}$ and $\mathbf{M}$ are the induced electric and magnetic polarisation in the medium. As the medium used in this Thesis is nonmagnetic, $\mathbf{M} = 0$.

A.1 Neutral medium

To describe light-matter interaction in a neutral medium, equation (A.1) has to be rewritten according to:

$$\begin{aligned} \nabla \times \nabla \times \mathbf{E} &= \nabla \times \left(-\frac{\partial \mathbf{B}}{\partial t} \right) = -\frac{\partial}{\partial t} \left(\nabla \times \mathbf{B} \right) = \{\mathbf{M} = 0\} = -\mu_0 \frac{\partial}{\partial t} \left(\nabla \times \mathbf{H} \right) = \\ &= \{\mathbf{J} = 0\} = -\mu_0 \frac{\partial}{\partial t} \left(\frac{\partial \mathbf{D}}{\partial t} \right) = -\mu_0 \frac{\partial^2}{\partial t^2} \left(\varepsilon_0 \mathbf{E} + \mathbf{P} \right) = \left\{ \mu_0 \varepsilon_0 = \frac{1}{c^2} \right\} = \\ &= -\frac{1}{c^2} \frac{\partial^2 \mathbf{E}}{\partial t^2} - \mu_0 \frac{\partial^2 \mathbf{P}}{\partial t^2} \end{aligned} \tag{A.7}$$

If then the relation

$$\nabla \times \nabla \times \mathbf{E} = \nabla \left(\nabla \cdot \mathbf{E} \right) - \nabla^2 \mathbf{E} = -\nabla^2 \mathbf{E} \tag{A.8}$$

(valid in a medium with no charge density) is used, equation (A.7) can be written like the following, also known as the wave equation:

$$\nabla^2 \mathbf{E} = \frac{1}{c^2}\frac{\partial^2 \mathbf{E}}{\partial t^2} + \mu_0 \frac{\partial^2 \mathbf{P}}{\partial t^2} \tag{A.9}$$

The wave equation describes how the electric field and the hereby induced polarisation in a medium change. If the optical frequency is far from the resonances of the medium, $\mathbf{P}$ and $\mathbf{E}$ are related according to:

$$\mathbf{P} = \varepsilon_0 \left(\chi^{(1)}\mathbf{E} + \chi^{(2)}\mathbf{E}^2 + \chi^{(3)}\mathbf{E}^3 + \dots \right) \tag{A.10}$$

As the nonlinear effect of primary importance is nonlinear refraction, it is enough to include only the third-order nonlinear contribution, governed by $\chi^{(3)}$. The induced polarisation then consists of two parts

$$\mathbf{P}(\mathbf{r},t) = \mathbf{P}_L(\mathbf{r},t) + \mathbf{P}_{NL}(\mathbf{r},t) \tag{A.11}$$

If this is inserted into (A.9), the wave equation now looks like [69]

$$\nabla^2 \mathbf{E} - \frac{1}{c^2}\frac{\partial^2 \mathbf{E}}{\partial t^2} = \mu_0 \left(\frac{\partial^2 \mathbf{P}_L}{\partial t^2} + \frac{\partial^2 \mathbf{P}_{NL}}{\partial t^2} \right) \tag{A.12}$$

Before equation (A.12) can be solved, it is necessary to make some simplifying assumptions. Since $\mathbf{P}_{NL}$ is small compared to $\mathbf{P}_L$, it can be treated as a small perturbation. The optical field is also assumed to maintain its polarisation along the propagation direction, which means that a scalar expression can be used. The optical field is finally considered to be quasi-monochromatic, i.e. the spectral width $\Delta\omega$ is much less than the central optical frequency ω_0, or mathematically $\frac{\Delta\omega}{\omega_0} \ll 1$. The pulses are then significantly longer than one optical cycle and it is enough to only study the slowly varying amplitude of the envelope, instead of the swiftly varying electric field. In the visible region this corresponds to pulses longer than ~ 0.1 ps [70]. With the above mentioned approximations, the resulting expression for the slowly varying envelope of the electric field is:

$$\frac{\partial A}{\partial z} + \beta_1 \frac{\partial A}{\partial t} + \frac{i\beta_2}{2}\frac{\partial^2 A}{\partial t^2} + \frac{\alpha}{2}A = i\gamma |A|^2 A \tag{A.13}$$

with the nonlinear parameter γ defined as

$$\gamma = \frac{n_2 \omega_0}{c A_{eff}} \tag{A.14}$$

A_{eff} is the effective area of the beam. The parameters β_1 and β_2 arise due to the frequency dependence of the mode-propagation constant β, according to the Taylor expansion

$$\begin{aligned} \beta(\omega) &= n(\omega)\frac{\omega}{c} = \beta_0 + \left(\frac{d\beta}{d\omega}\right)_{\omega=\omega_0} (\omega - \omega_0) + \\ &+ \frac{1}{2}\left(\frac{d^2\beta}{d\omega^2}\right)_{\omega=\omega_0} (\omega - \omega_0)^2 + \dots \end{aligned} \tag{A.15}$$

and are expressed as:

$$\begin{aligned} \beta_1 &= \frac{d\beta}{d\omega} \\ \beta_2 &= \frac{d^2\beta}{d\omega^2} \end{aligned} \tag{A.16}$$

β_2 causes a dispersion of the group velocity within the pulse and hence is responsible for a temporal stretching. For a more thorough description of dispersive and nonlinear effects, see sections 2.2 and 2.3. Equation (A.13) is often referred to as the nonlinear Schrödinger equation (NLS) and is valid for pulses of picosecond duration. However, for shorter pulses it has to be modified [71].

For ultrashort pulses, i.e. with a duration of less than 1 ps, the spectral width is broad enough to include some additional terms [72][73]-[82]. In general, an effect due to the delayed Raman vibrational response of a medium should be included. But since argon has a very fast response time compared to the pulse duration, it can be neglected. Two effects that however can not be neglected in this context are third-order dispersion and self-steepening, see further sections 2.2.2 and 2.3.2. If these effects are added to equation (A.13), together with a frame of reference moving with the pulse at the group-velocity v_g, according to

$$T = t - \frac{z}{v_g} \equiv t - \beta_1 z \tag{A.17}$$

the resulting propagation equation is:

$$\frac{\partial A}{\partial z} + \frac{\alpha}{2}A + \frac{i\beta_2}{2}\frac{\partial^2 A}{\partial T^2} - \frac{\beta_3}{6}\frac{\partial^3 A}{\partial T^3} = i\gamma\left[|A|^2 A + \frac{i}{\omega_0}\frac{\partial}{\partial T}\left(|A|^2 A\right)\right] \tag{A.18}$$

valid for pulses as short as $\sim$ 10 fs [83]. Here A is normalised such that $|A|^2$ represents the optical power [84]. If, in addition, the time scale and pulse amplitude are normalised according to

$$\tau = \frac{T}{T_0} \tag{A.19}$$

$$U(z,\tau) = \frac{1}{\sqrt{P_0}}A(z,\tau) \tag{A.20}$$

where T_0 and P_0 represent the input pulse duration (at $1/e^2$-intensity point) and peak power respectively, equation (A.18) becomes

$$\begin{aligned} \frac{\partial U}{\partial z} &= -i\frac{sgn(\beta_2)}{2L_D}\frac{\partial^2 U}{\partial \tau^2} + \frac{sgn(\beta_3)}{6L_D'}\frac{\partial^3 U}{\partial \tau^3} + \\ &+ i\frac{1}{L_{NL}}\left[|U|^2 U + is\frac{\partial}{\partial \tau}\left(|U|^2 U\right)\right] \end{aligned} \tag{A.21}$$

L_D, L_D' and L_{NL} are length scales, governing the relative importance of the dispersive and nonlinear effects, defined according to:

$$L_D = \frac{T_0^2}{|\beta_2|} \tag{A.22}$$

$$L_D' = \frac{T_0^3}{|\beta_3|} \tag{A.23}$$

$$L_{NL} = \frac{1}{\gamma P_0} \tag{A.24}$$

while the parameter s governs the effect of self-steepening [39][40]

$$s = \frac{1}{\omega_0 T_0} \tag{A.25}$$

A.2 Quantum mechanical description of tunnel ionisation

A.2.1 Ionisation by a static electric field

The electronic motion in atoms can generally be described by the time-independent Schrödinger equation, which for a spherically symmetric potential is written as:

$$\left\{-\frac{\hbar^2}{2m}\nabla^2 + V(r)\right\}\Psi(r) = E\Psi(r) \tag{A.26}$$

Due to the spherical symmetry, the Schrödinger equation is often separated in spherical polar coordinates, but if the central potential is the Coulomb potential

$$V(r) = -\frac{Ze^2}{(4\pi\varepsilon_0)\, r} \tag{A.27}$$

(as is the case for hydrogenic atoms) it can also be separated in parabolic coordinates. This treatment is for example useful when the atom is subject to an external electric field. The parabolic coordinates (ξ, η, ϕ) are related to the Cartesian coordinates (x, y, z) and the spherical polar coordinates (r, θ, ϕ) through:

$$x = \sqrt{\xi\eta}\cos\phi \tag{A.28}$$
$$y = \sqrt{\xi\eta}\sin\phi \tag{A.29}$$
$$z = \frac{1}{2}(\xi - \eta) \tag{A.30}$$
$$r = \frac{1}{2}(\xi + \eta) \tag{A.31}$$
$$\xi = r + z = r(1 + \cos\theta) \tag{A.32}$$
$$\eta = r - z = r(1 - \cos\theta) \tag{A.33}$$
$$\phi = \tan^{-1}\left(\frac{y}{x}\right) \tag{A.34}$$

with $0 \leq \xi \leq \infty$, $0 \leq \eta \leq \infty$, $0 \leq \phi \leq 2\pi$ [85]. Expressed in parabolic coordinates, the Schrödinger equation is:

$$-\frac{\hbar^2}{2\mu}\left\{\frac{4}{\xi+\eta}\left[\frac{\partial}{\partial\xi}\left(\xi\frac{\partial}{\partial\xi}\right) + \frac{\partial}{\partial\eta}\left(\eta\frac{\partial}{\partial\eta}\right)\right] + \frac{1}{\xi\eta}\frac{\partial^2}{\partial\phi^2}\right\}\Psi -$$
$$-\frac{2Ze^2}{(4\pi\varepsilon_0)(\xi+\eta)}\Psi = E\Psi \tag{A.35}$$

where $\mu = \frac{m_e m_N}{m_e + m_N}$ is the reduced mass of the electron and the nucleus. The electric field changes the potential felt by the electron according to:

$$V = -\frac{Ze^2}{(4\pi\varepsilon_0)\, r} + e\mathscr{E}z = -\frac{2Ze^2}{(4\pi\varepsilon_0)(\xi+\eta)} + \frac{1}{2}e\mathscr{E}(\xi - \eta) \tag{A.36}$$

where $\mathscr{E}$ represents a *static* electric field, applied along the z-direction. The potential hence approaches $-\infty$ at the site of the nuclues, as well as for large negative values of z; two areas separated by a barrier. In other words, there exists a finite possibility that the electron, which initially is in a bound state, will leave the atom by tunneling through this potential barrier. The phenomenon is therefore known as tunneling ionisation.

To obtain an approximate expression for the rate of ionisation, the probability to find the electron under the potential barrier must be calculated. This requires knowledge about the perturbed ground state wave function Ψ_0^p, provided through the time-independent Schrödinger equation, treating the external electric field as a perturbation. The following derivation can be found in reference [86].

The Schrödinger equation for a hydrogenic atom in the presence of a static electric field is:

$$\begin{aligned} - & \frac{\hbar^2}{2\mu}\left\{\frac{4}{\xi+\eta}\left[\frac{\partial}{\partial\xi}\left(\xi\frac{\partial}{\partial\xi}\right)+\frac{\partial}{\partial\eta}\left(\eta\frac{\partial}{\partial\eta}\right)\right]+\frac{1}{\xi\eta}\frac{\partial^2}{\partial\phi^2}\right\}\Psi - \\ - & \left(\frac{2Ze^2}{(4\pi\varepsilon_0)(\xi+\eta)}+\frac{1}{2}e\mathscr{E}(\xi-\eta)\right)\Psi = E\Psi \end{aligned} \tag{A.37}$$

If the variables are separated by assuming that the eigenfunctions are expressed by

$$\Psi(\xi,\eta,\phi) = f(\xi)\,g(\eta)\,\Phi(\phi) \tag{A.38}$$

the following equations, in atomic units, are obtained:

$$\frac{1}{\Phi}\frac{d^2\Phi}{d\phi^2} = -m^2 \tag{A.39}$$

$$\left[\frac{d}{d\xi}\left(\xi\frac{d}{d\xi}\right)+\left(\frac{1}{2}E\xi-\frac{m^2}{4\xi}-\frac{1}{4}\mathscr{E}\xi^2+v_1\right)\right]f = 0 \tag{A.40}$$

$$\left[\frac{d}{d\eta}\left(\eta\frac{d}{d\eta}\right)+\left(\frac{1}{2}E\eta-\frac{m^2}{4\eta}+\frac{1}{4}\mathscr{E}\eta^2+v_2\right)\right]g = 0 \tag{A.41}$$

The constants v_1 and v_2 fulfil the condition $v_1+v_2=Z$, where Z represents the atomic number. The field strength considered is $\mathscr{E}\ll 1$. Equation (A.39) is easily solved, according to

$$\Phi_m(\phi) = \frac{1}{\sqrt{2\pi}}e^{im\phi} \tag{A.42}$$

where m is the magnetic quantum number, $m=0,\pm1,\pm2,\ldots$. If the substitutions $f=\xi^{-1/2}F$, $g=\eta^{-1/2}G$ are made in equations (A.40) and (A.41), two one-dimensional Schrödinger equations are obtained, with the energy $E/4$ and the potentials V_1 and V_2 according to:

$$-\frac{1}{2}\frac{d^2F}{d\xi^2}+V_1(\xi)\,F = \frac{E}{4}F \tag{A.43}$$

$$-\frac{1}{2}\frac{d^2G}{d\eta^2}+V_2(\eta)\,G = \frac{E}{4}G \tag{A.44}$$

$$V_1(\xi) = \frac{m^2-1}{8\xi^2} - \frac{v_1}{2\xi} + \frac{\mathscr{E}\xi}{8} \quad (A.45)$$

$$V_2(\eta) = \frac{m^2-1}{8\eta^2} - \frac{v_2}{2\eta} - \frac{\mathscr{E}\eta}{8} \quad (A.46)$$

An expression for the unperturbed ground state wave function that satisfies equations (A.43) and (A.44) with $E = -1/2$, as well as equations (A.45) and (A.46) with $\mathscr{E} = 0$ and $v_1 = v_2 = 1/2$, is:

$$\Psi_0 = \pi^{-1/2}(\xi\eta)^{-1/2} F_0(\xi) G_0(\eta) \quad (A.47)$$

with

$$F_0(\xi) = \xi^{1/2}\exp(-\xi/2) \quad (A.48)$$

$$G_0(\eta) = \eta^{1/2}\exp(-\eta/2) \quad (A.49)$$

This means that an expression for the perturbed ground state wave function of the form

$$\Psi_0^p = \pi^{-1/2}(\xi\eta)^{-1/2} F(\xi) G(\eta) \quad (A.50)$$

should be sought.

The region of interest for calculating the ionisation rate is represented by finite values of x and y, while $z \to -\infty$. In parabolic coordinates, this corresponds to small values of ξ and large values of η, according to equations (A.28)-(A.30). For $\mathscr{E} \ll 1$, the following approximation can be made for all ξ:

$$F(\xi) \simeq F_0(\xi) \quad (A.51)$$

For large values of η however, the WKB-approximation has to be employed to obtain an approximate expression for $G(\eta)$. WKB is an acronym for Wentzel, Kramers and Brillouin, who developed this theory in 1926 [87]. The WKB-approximation can be used when the potential energy is a slowly varying function of position, i.e. only changes slightly over the de Broglie wavelength of the particle. This is the case for $V_2(\eta)$. If the WKB-approximation is applied to equation (A.44) for large values of η, $G(\eta)$ can be approximated by:

$$G(\eta) \simeq A\,|p(\eta)|^{-1/2}\exp\left[i\int_{\eta_0}^{\eta} p\left(\eta'\right)d\eta'\right] \quad (A.52)$$

$$p(\eta) = \left\{2\left[\frac{E}{4} - V_2(\eta)\right]\right\}^{1/2} = \left[-\frac{1}{4} + \frac{1}{4\eta^2} + \frac{1}{2\eta} + \frac{1}{4}\mathscr{E}\eta\right]^{1/2} \quad (A.53)$$

because $E = -1/2$. $p(\eta)$ is expressed in atomic units and is a positive complex quantity in the region of interest. The value of the constant A is given by:

$$A = [\eta_0|p(\eta_0)|]^{1/2}\exp(-\eta_0/2) \quad (A.54)$$

For a more complete derivation, see [88]. To account for large values of η, $G(\eta)$ in the limit $\eta \to +\infty$ must be calculated. With the expression for A inserted,

$|G(\eta)|$ looks like:

$$|G(\eta)| = \eta_0^{1/2} \left| \frac{p(\eta_0)}{p(\eta)} \right|^{1/2} \exp\left[-\int_{\eta_0}^{\eta} \left| p\left(\eta'\right) \right| d\eta' - \eta_0 \right] \quad \text{(A.55)}$$

After some approximations, see [89], the final expression for large values of η is

$$|G(\eta)| \simeq \frac{2}{\mathscr{E}^{1/2} (\mathscr{E}\eta - 1)^{1/4}} \exp\left(-\frac{1}{3\mathscr{E}} \right) \quad \text{(A.56)}$$

which gives the following expression for the perturbed ground state wave function:

$$\begin{aligned} \Psi_0^p &= \pi^{-1/2} (\xi\eta)^{-1/2} F_0(\xi) G(\eta) = \\ &= \frac{1}{\pi^{1/2}} \frac{2}{\mathscr{E}^{1/2}\eta^{1/2} (\mathscr{E}\eta - 1)^{1/4}} \exp\left(-\frac{1}{3\mathscr{E}} \right) \exp(-\xi/2) \end{aligned} \quad \text{(A.57)}$$

The ionisation rate equals the number of electrons passing through a plane perpendicular to the z-axis per unit time as $z \to -\infty$ and has the following mathematical formulation:

$$W_{ion} = \int_0^{2\pi} d\phi \int_0^{\infty} d\rho\rho \left|\Psi_0^p\right|^2 v_z \quad \text{(A.58)}$$

Here v_z is the z-component of the electron velocity and $\rho = \left(x^2 + y^2\right)^{1/2} = (\xi\eta)^{1/2}$. For a fixed value of $-z$, where $|z|$ is large, the value of η is fixed since the significant values of ξ are small. The following substitution can therefore be made:

$$d\rho = \frac{1}{2}\xi^{-1/2}\eta^{1/2} d\xi \quad \text{(A.59)}$$

Equation (A.58) then becomes

$$W_{ion} = (2\pi)\frac{1}{2} \int_0^{\infty} \eta \left|\Psi_0^p\right|^2 v_z d\xi \quad \text{(A.60)}$$

since Ψ_0^p is independent of ϕ. For large values of $|z|$, the motion of the electron is considered to be classical and a mathematical expression can be derived, using the conservation of energy

$$E = \frac{1}{2} v_z^2 + \mathscr{E} z \quad \text{(A.61)}$$

With $E = -1/2$ and $-z \simeq \eta/2$ the expression is

$$v_z = (\mathscr{E}\eta - 1)^{1/2} \quad \text{(A.62)}$$

If equations (A.57) and (A.62) are inserted in equation (A.60), the final expression for the ionisation rate becomes:

$$W_{ion}(\mathscr{E}) = \frac{4}{\mathscr{E}} \exp\left(-\frac{2}{3\mathscr{E}} \right) \quad \text{(A.63)}$$

[89].

A.2.2 Ionisation by an alternating electric field

The derivation of the ionisation rate in the previous section is only valid for a static electric field. However, in most real cases, the electric field is usually varying in time with the frequency ω. To derive an expression for the ionisation rate for an alternating electromagnetic field, some approximations are often made. If the strength of the field is much smaller than the intraatomic electric field, the mean time of ionisation is large in comparison with characteristic atomic times. If, in addition, the frequency of the field is much less than the tunneling frequency, $\omega_t = \frac{E_{laser}}{\sqrt{2I_p}}$, the external field can be considered constant during the time the electron tunnels through the barrier. The last condition is often referred to as the adiabatic approximation and is valied for $\gamma \ll 1$, see equation (2.13). The calculation of the ionisation rate then reduces to simply averaging the ionisation rate for a constant field over a period of the external field. According to Ammosov, Delone and Kraĭnov in 1986 (the ADK-theory), the ionisation rate for a linearly polarised, alternating electromagnetic field can be written in the following form (in atomic units):

$$\begin{aligned} W_{ion,linear}\left(\mathscr{E},\omega\right) &= \left(\frac{3\mathscr{E}}{\pi\mathscr{E}_0}\right)^{1/2} \times \left|C_{n^*l^*}\right|^2 E \frac{\left(2l+1\right)\left(l+\left|m\right|\right)!}{2^{\left|m\right|}\left(\left|m\right|\right)!\left(l-\left|m\right|\right)!}\left(\frac{2\mathscr{E}_0}{\mathscr{E}}\right)^{2n^*-\left|m\right|-1} \times \\ &\times \exp\left(\frac{-2\mathscr{E}_0}{3\mathscr{E}}\right) \end{aligned} \tag{A.64}$$

[38]. Here $\mathscr{E}_0 = \left(2E\right)^{3/2}$, $n^* = Z\left(2E\right)^{-1/2}$, E is the electron energy, Z is the charge of the resulting ion and $\mathscr{E}$ is the amplitude of the external field. l and m are the orbital and magnetic quantum number respectively. The factor $\left(\frac{3\mathscr{E}}{\pi\mathscr{E}_0}\right)^{1/2}$ appears from averaging over a period of the external field and $\left(2\mathscr{E}_0/\mathscr{E}\right)^{2n^*-\left|m\right|-1}$ is a factor which takes the Coulomb interaction into account. The expression for the dimensionless constant $\left|C_{nl}\right|^2$ is known only for the hydrogen atom, but by applying the asymptotic Stirling formula it can be written as

$$\left|C_{n^*l^*}\right|^2 = \frac{1}{2\pi n^*}\left(\frac{4e^2}{n^{*2}-l^{*2}}\right)^{n^*}\left(\frac{n^*-l^*}{n^*+l^*}\right)^{l^*+1/2} \tag{A.65}$$

for an arbitrary atom. $n^* = n-\delta_l$ and $l^* = l-\delta_l$ represent the effective quantum numbers, which take the quantum defect $\delta_l = n - \left(2E\right)^{-1/2}$ into consideration [34]. If the expression for $\left|C_{n^*l^*}\right|^2$ is inserted into the expression for the ionisation rate, equation (A.64), it can be seen that the maximum rate is obtained for $\left|m\right| = 0$.

Equation (A.64) was derived for the case of linearly polarised light. In some situations, however, the incident field is elliptically polarised according to:

$$\mathscr{E}\left(t\right) = \mathscr{E}\left(e_x \cos\omega t \pm \varepsilon e_y \sin\omega t\right) \tag{A.66}$$

$0 \geq \varepsilon \leq 1$ where $\varepsilon = 1$ represents circular polarisation. The ionisation rate for a circularly polarised, alternating electromagnetic field differs somewhat from the linear case and can be written (also in atomic units) according to [90]:

$$W_{ion,circular} = \left(\frac{3\mathscr{E}}{\pi\mathscr{E}_0}\right)^{-1/2} W_{ion,linear} \tag{A.67}$$

Since $\mathscr{E} \ll E$, the ionisation rate is always higher than for linear polarisation. However, the corresponding field strength is a factor of $\frac{1}{2}$ smaller for the same intensity [91].

Appendix B

The refractive index

To be able to simulate the dispersive and nonlinear effects a pulse experiences from a certain medium, the refractive index has to be known. For *solid* materials the Sellmeier equation has been used, according to:

$$n^2 = 1 + \frac{B_1\lambda^2}{\lambda^2 - C_1} + \frac{B_2\lambda^2}{\lambda^2 - C_2} + \frac{B_3\lambda^2}{\lambda^2 - C_3} \tag{B.1}$$

where B_n and C_n are constants, characteristic for a specific material. In equation (B.1), λ should be expressed in μm [45]. The solid material used in this Thesis is sapphire, with the following constants [92]:

Table B.1 *Material constants for sapphire*

B1	1.43134930
B2	0.650547130
B3	5.34140210
C1	0.00527992610
C2	0.0142382647
C3	325.017834

For *gases* on the other hand, the refractive index is expressed by:

$$n^2 = 1 + k_1\left(1 + \frac{k_2}{\lambda^2} + \frac{k_3}{\lambda^4} + \frac{k_4}{\lambda^6} + \frac{k_5}{\lambda^8} + \frac{k_6}{\lambda^{10}} + \dots\right) \tag{B.2}$$

Here λ is expressed in Å instead and $k_1 - k_6$ denote constants. The gas used is argon, with the following values [93]:

Table B.1 *Specific constants for argon*

k_1	$5.547 \cdot 10^{-4}$
k_2	$5.15 \cdot 10^{5}$
k_3	$4.19 \cdot 10^{11}$
k_4	$4.09 \cdot 10^{17}$
k_5	$4.32 \cdot 10^{23}$
k_6	–

As already has been stated in this Thesis, for high enough intensities the nonlinear refractive index of a medium must also be considered. For sapphire and argon this is [94][95]:

Table B.1 *The nonlinear refractive index,* n_2 $(\mathrm{m}^2/\mathrm{W})$

Al_2O_3	$3.2 \cdot 10^{-20}$
Ar	$0.980 \cdot 10^{-23}$